





3 1293 01022 2598

This is to certify that the

dissertation entitled

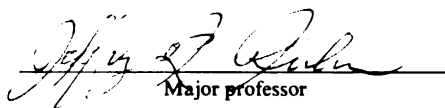
**Study of Diffuse  
Light in CD  
Galaxy Clusters**

presented by

**Xania Scheick**

has been accepted towards fulfillment  
of the requirements for

Ph.D. degree in Physics

  
Major professor

Date Oct. 22, 1993

# LIBRARY

## Michigan State University

**PLACE IN RETURN BOX** to remove this checkout from your record.  
**TO AVOID FINES** return on or before date due.

DATE DUE	DATE DUE	DATE DUE
_____	_____	_____
_____	_____	_____
_____	_____	_____
_____	_____	_____
_____	_____	_____
_____	_____	_____
_____	_____	_____

**STUDY OF DIFFUSE LIGHT IN CD GALAXY CLUSTERS**

By

Xania Scheick

A DISSERTATION

Submitted to

Michigan State University

in partial fulfillment of the requirements

for the degree of

**DOCTOR OF PHILOSOPHY**

Department of Physics and Astronomy

1993



## **ABSTRACT**

### **STUDY OF DIFFUSE LIGHT IN CD GALAXY CLUSTERS**

By

Xania Scheick

Conventionally, the gravitational potential of galaxy clusters has been mapped using the galaxies themselves or X-rays as test particles. Using the intra-cluster medium or diffuse light instead has the obvious advantage in sheer number of particles, i.e. better counting statistics. Analysis of diffuse light in two cD clusters (A2670 and A2029) is described. Deep R-band CCD images of these clusters were procured at the KPNO 36" and 2.1m telescopes. On large scales, the diffuse light is well fit by a de Vaucouleurs' profile. This "smoothness" is suprising in light of current cluster evolution theory which relies on violent interactions among cluster members. Thus we are motivated to study the diffuse light on small scales, expecting a priori to see clumpiness in the medium due to collisional or tidal stripping mechanisms or the affects of dynamical friction.

Using a statistical approach, we have determined the source of the diffuse light to be numerous low luminosity objects. The clumpiness of the diffuse light in both clusters is described by autocorrelations of the residual images (after diffuse light has been removed). From this analysis, we can determine a spatial scale of the clumps and attempt to place some constraints on the faint end of the cluster luminosity function. For A2670, we compute a differential luminosity function in the cluster center that suggests real differences in the luminosity function within

the cluster center from a universal cluster luminosity function. We measure the V-R color of the cD and cluster galaxies and the color gradient across the halo of A2670. In A2029, we find structures associated with five galaxies suggestive of wakes, i.e. the gravitational response of the medium to galactic passage. The apparent lack of significant small-scale structure poses a curious problem for cluster evolution models.

For those responsible: *you know who you are.*

## ACKNOWLEDGEMENTS

I would like to acknowledge and thank my advisor, Jeff Kuhn, for giving the tools to complete this project. I would like to beg his forgiveness for leading a separate life apart from physics; if I had devoted all my passion to science, I would have saved him alot of money, headaches, etc, but would have gone insane. I should also thank Juan Uson and Steve Boughn for help formulating the original thesis and for many conversations afterwards. Many thanks to Debbie Benedict who was always ready to hear my gossip when I couldn't focus on the computer screen. I can't forget the perpetrators of my existence for brainwashing me to "get educated", my sibling who has just started his graduate program, and all my furry friends.

## TABLE OF CONTENTS

<b>LIST OF TABLES</b> .....	viii
<b>LIST OF FIGURES</b> .....	ix
<b>INTRODUCTION</b> .....	1
1.1 Clusters of Galaxies .....	1
1.2 CD Galaxies .....	2
1.3 Cluster Evolution Theories: Origin of Diffuse Light .....	6
1.3.1 Cooling Flows, Mergers, or a Primordial Origin .....	6
1.3.2 Color, Velocity Dispersion, and CD Formation .....	15
1.4 Previous Diffuse Light Measurements .....	19
1.5 This Investigation .....	21
<b>OBSERVATIONS AND DATA REDUCTION</b> .....	24
2.1 Observations .....	24
2.1.1 A2670 .....	24
2.1.2 A2029 .....	25
2.2 Data Reduction .....	26
2.2.1 Standard Processing .....	26
2.2.2 Shifting and Tessellating .....	27
2.2.3 General Photometry and PSF subtraction .....	30
<b>ANALYSIS</b> .....	32
3.1 A2670 .....	32

3.1.1 Diffuse Light Profile .....	32
3.1.2 Number Density and Luminosity Function .....	43
3.1.3 Autocorrelation .....	44
3.1.4 Color .....	53
3.1.5 Wakes .....	54
3.2 A2029 .....	57
3.2.1 Diffuse Light Profile .....	57
3.2.2 Autocorrelation .....	60
3.2.3 Wakes .....	69
<b>DISCUSSION .....</b>	<b>76</b>
4.1 A2670 .....	76
4.2 A2029 .....	87
4.3 Concluding Remarks .....	89
<b>LIST OF REFERENCES .....</b>	<b>90</b>

**LIST OF TABLES**

**Table 1: Simple Wake Characteristics .....75**

## LIST OF FIGURES

Figure 1: Gray-scale Image of the Central 10 arcmin <sup>2</sup> of A2670 .....	34
Figure 2: Contour Map of the Inner 1 arcmin <sup>2</sup> of A2670 .....	35
Figure 3: Outer R-band Diffuse Light Profile in A2670 .....	36
Figure 4a: De Vaucouleurs' fit to R-band Diffuse Light Profile in A2670 .....	38
Figure 4b: De Vaucouleurs' fit to V-band Diffuse Light Profile in A2670 .....	39
Figure 5: Total R-band Cluster Light & Diffuse Light in A2670 .....	40
Figure 6: Square of the Variance per Radial Bin in A2670 Residual Image .....	42
Figure 7: Object Number Density & Scaled Diffuse Light in A2670 .....	45
Figure 8: Differential Luminosity Function for A2670 Inner Region .....	46
Figure 9: R-band Autocorrelations of Inner & Outer Regions of A2670 .....	48
Figure 10: V-band Autocorrelations of A2670 Data & Fit Subtracted Images ..	49
Figure 11: Autocorrelations of 50 & 100 Masked Gaussian Objects .....	51
Figure 12a: Histogram of V-R Color of Objects in A2670 .....	55
Figure 12b: Histogram of V-R Color of Objects in Background Frame .....	55
Figure 13: V-R Color of the A2670 Diffuse Light .....	56
Figure 14: Gray-scale Image of the Central 4.5 arcmin <sup>2</sup> of A2029 .....	58
Figure 15: Contour Map of the Inner 1 arcmin <sup>2</sup> of A2029 .....	59
Figure 16: Our and UBK's R-band Diffuse Light Profile of A2029 .....	61
Figure 17: Autocorrelations of the Inner Region of A2029 .....	63
Figure 18: Autocorrelations of the Outer Region of A2029 .....	64
Figure 19: Autocorrelations of the Inner Region of A2670 .....	67



Figure 20: Autocorrelations of the Outer Region of A2670 .....	68
Figure 21: Contour Maps of Candidate Wakes, 1. ....	70
Figure 21 (cont'd): Candidate 2. ....	71
Figure 21 (cont'd): Candidate 3. ....	72
Figure 21 (cont'd): Candidate 4. ....	73
Figure 21 (cont'd): Candidate 5. ....	74
Figure 22a: De Vaucouleurs' Fit to Oemler's A2670 Diffuse Light Measurement	78
Figure 22b: Oemler's & de Vaucouleurs' Fit to Our Diffuse Light Measurement	79

## CHAPTER 1

# INTRODUCTION

### 1.1 Clusters of Galaxies

Even though only  $\sim 5\%$  of the galaxies are contained in groups and clusters whose space density is larger than one galaxy per cubic megaparsec, clusters are distinctly visible against the background of galaxies making up our present-epoch universe. Abell (1958) catalogued the most dense of these during the original Palomar survey. A typical Abell cluster contains 100 galaxies with a luminosity range of two orders of magnitude over an extent of several megaparsecs.

Because of their high surface densities and large number of bright galaxies, galaxy clusters are identified out to distances comparable to the horizon of the universe making them a valuable tool for cosmology (Hubble 1936, Zwicky 1938). Early research centered on the measurements of standard candles, such as luminosity of the brightest cluster members (BCMs) or the characteristic luminosity  $L_*$  in the cluster luminosity function (LF), and standard metrics, such as radii of cluster galaxies or that of the cluster as a whole. Research before the 1970s concerned morphological description of sizes, shapes, and galaxy content of clusters and the use of these parameters in cosmological investigations.

The next generation of research concerned galaxy evolution. Certain clusters contain "supergalaxies" like none seen amongst the field galaxies. The general population of galaxies in clusters is predominately (60%) elliptical and gas-free disk

systems (S0s), whereas the field galaxies are mainly spirals (70%). The spirals in clusters have  $\sim 0.2$  mag larger B-V color than those in the field. The cluster environment also contains a pervasive, hot intergalactic gas observed by its X-ray radiation. The research emphasis since the 1970s has been to determine how the cluster galaxies evolve and affect the evolution of the cluster as a whole. Clusters of galaxies are excellent laboratories for studying the dynamical evolution of galaxies, for although the relative velocities are large (thus the timescales for interaction are small), the galaxy densities are high, and therefore the probability for interaction is substantially greater than in the field.

## 1.2 CD Galaxies

W. W. Morgan called attention to the bright elliptical galaxies surrounded by an extensive amorphous stellar envelope (Morgan 1958, Matthews et al. 1964, Morgan & Lesh 1965), which were called D galaxies, meaning "dustless". The largest and thus most luminous of these, with an extent 3-4 times that of the largest S0s in the cluster, was called a supergiant D galaxy or cD galaxy. The designation "c" was originally coined for stars with unusually narrow H lines which are now understood to be superluminous (Tonry 1987).

The large size is only the primary characteristic of cD galaxies, but it is the one used in classifying clusters (Struble & Rood 1982). Unfortunately there has never been universal agreement on the proper use of the terms D and cD. Some observers, including Morgan & Lesh, use secondary properties (like the cD is the BCM and is centrally located in the cluster) to define cD-ness, but neither of these attributes is necessary and sufficient to identify a cD.

A brief description of these secondary characteristics is as follows: cDs usually

reside in the cores of rich, regular clusters (Oemler 1974, 1976); however cDs and Ds are sometimes found in irregular clusters at local density enhancements. The cD envelopes are often extremely large in extent, and the cD is frequently found at the kinematical center of its cluster (Quintana & Lawrie 1982). They often are very "flat" galaxies and are aligned to a flattened distribution of cluster members (Carter & Metcalfe 1980, Dressler 1981, Binggeli 1982); however as with other giant ellipticals, their flattening is not primarily due to rotation (Faber et al. 1977, Dressler 1979). Anywhere from 25-50% have multiple nuclei (Rood & Leir 1979, Hoessel 1980, Schneider et al. 1983).

Velocity dispersion measurements of D and cD galaxies show flat or rising profiles with increasing radius progressing well into the low surface brightness envelopes. Carter et al. (1985) present rotation and velocity dispersion measurements in the halos of one dumb-bell and two single nucleus cDs out to roughly 35" or 24 R mag/arcsec<sup>2</sup>. The two cDs show some indication that the velocity dispersion increases for radii greater than 20" though there are large errors associated with the outermost points. The increase is from about 300 km/s at the nucleus to 500 km/s at their last data point. Dressler (1979) obtained spectra of the envelope of A2029 out to 100 kpc (roughly 45"). He reports that the velocity dispersion increases with radii from roughly 370 to 510 km/s in this region. The profile is smooth with the exception of a "bump" at 10 kpc which may be contamination from a nearby galaxy. This behavior, flat or rising velocity dispersion profiles, is not seen in normal ellipticals. This result suggests that the outer envelopes' dynamical states (i.e. the dynamics of the cluster orbits instead of the kinematics of the underlying galaxy) are influenced by the overall cluster potential.

Although not observed in all cD clusters, the following three characteristics are

thought by some researchers to indicate that the cD envelope is a separate entity from the cD itself: the velocity dispersion increase, the apparent inflection in the cD surface brightness profile at  $\sim 24\text{-}25 \text{ mag/arcsec}^2$ , and the success of a two component model (a normal elliptical with a "cluster-filling" component) fitting the latter profile. The break in the surface brightness profile at  $\sim 25 \text{ mag/arcsec}^2$  was first reported by Bahcall (1977) and Oemler (1976) as that point where the profile changes from  $\propto r^{-2}$  to  $r^{-1.6}$  where  $r$  is radius from the cluster center. Schombert (1987) works out cD profile morphology criteria: cDs all have properties of D galaxies (following  $r^{0.25}$  in the inner regions) with the addition of large extended envelopes, the onset of which occur when there is a change of slope at around  $24\text{-}25 \text{ mag/arcsec}^2$ . According to Schombert, there are many visually classified cDs without extended envelopes, as well as a few non-first-ranked galaxies with cD envelopes.

Tremaine (1989) suggests the use of the term "central galaxy" instead of cD to denote a galaxy at the bottom of a cluster potential basin as measured by the surface brightness of galaxies or X-ray surface brightness. Jones & Forman (1984) show that in most cases the potential minimum as measured from the maximum X-ray surface brightness coincides with the location of the brightest galaxy in the cluster core. Beers & Geller (1983) find that the potential minimum as marked by the local maximum in galaxy surface density is often occupied by a bright galaxy. Over 80% of the D and cD galaxies in the Beers & Geller sample are located at the the surface density maxima, and over 80% are the brightest galaxies in the cluster core. Faint D and cD galaxies are also located at the potential minimum, since their root-mean-square (RMS) velocity with respect to the cluster mean is smaller than that of typical galaxies in the cluster (Quintana & Lawrie 1982, Smith et al. 1985). Following Tremaine's definition, a central galaxy includes most galaxies

with extended envelopes or surface brightness profiles with relatively flat logarithmic slopes and those which are also usually brighter than typical galaxies and brighter than any in the potential basin. Although, Malumuth (1983), Schombert (1984), and others have pointed out that a galaxy looks distended because of the logarithmic slope of the surface brightness profile at the plate limit. This would then govern whether or not a galaxy looks as though it has a halo. Their work suggests that the cD core/halo distinction is not a real physical one.

The interiors of cD galaxies have properties similar to normal ellipticals (Thuan & Romanishin 1981), including velocity dispersion, mass-to-light ratios ( $M/L$ ), optical spectra and colors (therefore stellar populations), and densities (Faber et al. 1977, Dressler 1979, Malumuth & Kirshner 1981). Early aperture studies indicated that cDs have the colors of normal bright ellipticals (Lugger 1984 and references therein). Valentijn (1983) showed the existence of blue cD envelopes for five out of six cDs from multicolor surface photometry. Color gradient studies of high luminosity ellipticals are now quite extensive (e.g. Cohen 1986, Peletier et al. 1990, Mackie et al. 1990). Mackie et al. (1990) found small color gradients over the inner 20 kpc for a sample of 11 central dominant galaxies. Mackie (1992) has obtained deep  $g$  and  $r$  band CCD images of A2589, A2634, and A407 containing cDs or objects related to cDs. He finds no evidence of a color change at the surface brightness break that some think signifies the start of the cD envelope, nor are the envelope colors dramatically blue. In fact, for one object the colors become redder at larger radii. Schombert (1988) used the Palomar 1.5m with reimaging optics and an RCA CCD to obtain B-V profiles for three cDs (NGC 6034, A1767 G1 and A1413 G1). Errors in the colors at the envelopes are large ( $\pm 0.25$  mag), and the behavior of the gradients especially in the envelope is difficult to judge, but Schombert suggests

both a lack of strong color gradient and blue envelope colors in all three cDs. Upturns in color profiles (going redward with increasing radius) have been previously seen in a small number of galaxies. Red gradients are seen in  $\sim 40\%$  of McNamara & O'Connell's (1992) sample. A red envelope has been detected in a poor cluster cD (Maccagni et al. 1988) although there is some concern over the care taken in the analysis.

### **1.3 Cluster Evolution Theories: Origin of the Diffuse Light**

#### **1.3.1 Cooling Flows, Mergers, or a Primordial Origin**

There are three current models of cluster evolution which may explain the origin of the diffuse light. Cooling flow theory introduces the idea that radiative cooling of hot X-ray gas decreases its pressure and, then, this denser gas settles toward the center of the potential. If there is a galaxy at this location, the gas can collect until sufficient densities are obtained to start star formation (Fabian et al. 1984). There are merger models (Ostriker & Tremaine 1975; Ostriker & Hausman 1977; Hausman & Ostriker 1978; McGlynn & Ostriker 1980) in which a central dominant galaxy is formed and continues to grow by galactic interactions and cannibalism. The central mass distribution is also fed by material stripped from galactic halos by galactic collisions and/or tidal stripping. In this model and the cooling flow scenario, clusters are currently evolving, and the variety of cluster properties we observe now are characteristic of various stages of their evolution. The competing model might be called "primordial origin theory" (Merritt 1984a). Here the violent processes that are occurring at the present time in the merger models are most effective during the initial collapse of the cluster. The hypothesis is that all galaxies originally had large halos, which were stripped by the tidal fields created in the

cluster collapse. The cD halo remains unaffected because of its position in the cluster potential, except to receive the stripped material from the other galaxies. In this model, the cluster cDs are finished products—the timescales for mechanisms like dynamical friction and collisional stripping to significantly affect the cD being longer than the Hubble time.

The cooling time for gas in some clusters may be short enough that  $\sim 10^{12} M_{\odot}$  of gas may accumulate at the cluster center over a Hubble time (anywhere from 10 to 1000  $M_{\odot}/\text{yr}$  are observed). Efficient conversion of the gas into stars could create a bright central galaxy. However, the colors of most central galaxies are inconsistent with the substantial present star formation rate unless most of the stars are low-mass and therefore undetectable. In this case, the M/L should be high, whereas in fact central galaxies have the same M/L as normal ellipticals. Since the cDs are so much like normal ellipticals, one can conclude one of the following (Dressler 1984): i) the accretion is taking place onto a pre-existing galaxy and has not significantly altered its structure; ii) the accretion is directed towards a center of dark matter binding the cluster with core radius  $\sim 500$  kpc, but dissipation in the gas causes it to form a much more condensed structure; iii) a condensed structure in the dark matter, such as a "black pit" suggested by Blanford & Smarr (1984), forms a skeleton over which the cD is built from inflowing gas.

Blanford & Smarr (1984) attempt to explain the large number of fast-moving companion ellipticals found within  $\sim 10$  kpc of many cD galaxies. They propose that the dark binding material of the cluster actually has a much smaller radius ( $\sim 10$  kpc) than the core radius,  $\sim 500$  kpc, of the galaxy distribution. Binding these companion galaxies with such high orbital velocities would make the time scale for accretion by the cD quite long and would therefore explain why such multiple



systems are common. Observations of velocity dispersion profiles indicated that some cD galaxies do not contain such black pits, since the velocity dispersion at 10 kpc would have to rise to  $\sim 700$  km/s. Tonry's (1984) observations also seem to rule out black pits with core radii less than 12 kpc in A2199 (NGC 616) and A2634 (NGC 7720), which were the best candidates. Tonry's (1986) numerical simulations show that the orbits of galaxies remain highly elliptical as they are captured. Thus, these simulations are able to reproduce the proper frequency of such companions without an extremely concentrated distribution of dark matter.

A spectrophotometric study of cooling flow galaxies by McNamara & O'Connell (1989) show small anomalies such as UV excesses. McNamara & O'Connell (1992) present CCD imaging of 19 cooling flow galaxies out to about 30 kpc which display small color profile anomalies, such as bluer central colors, with respect to a sample of non-cooling-flow galaxies. While these results are interesting, interpretation of the anomalies is difficult due to the scatter in the correlations of cooling flow values, uncertainties in both metallicity levels and model predictions of mass drop-out positions. Some galaxies with cooling rates expected to display large spectral and photometric anomalies, e.g. IC 1101 in A2029 with  $360 M_{\odot}/\text{yr}$ , have normal elliptical spectra. The formation of envelopes via cooling flows would require preferential drop-out at large radii. Similar results were found by Romanishin (1987) for a smaller sample of cooling flow galaxies.

The strongest evidence for the dynamical evolution by mergers to date is the study of Hoessel & Schneider (1985), which found up to 48% have multiple nuclei (smaller galaxies seen projected on top of the luminosity profile 10-20 kpc from the center) and are assumed to be in the process of accretion. This level of multiplicity in BCMs is nearly an order of magnitude larger than that expected for chance

line-of-sight superpositions of galaxies within the isothermal core of a rich cluster (Tonry 1984). Schneider et al. (1983) show that multiplicity is peculiar to BCMs: only 5% of second- and third-ranked ellipticals are observed to have multiple nuclei. They also show that even though the density varies an order of magnitude for richness class 0 to 4 clusters, multiplicity is roughly independent of cluster richness. Considered naively, this result implies that evolution is more rapid in poorer clusters, which is not unreasonable since the evolution rates are expected to be  $\propto \sigma_v^{-2}$  where  $\sigma_v$  is cluster velocity dispersion (Merritt 1984a) which increases with cluster richness (Bahcall 1981). While the interaction cross-section may increase with the decrease in  $\sigma_v$ , the time between interactions also increases, and therefore the number of interactions/time will decrease. Hence, evolution may not necessarily be more rapid in poorer clusters, unless there are substantially more slow-moving galaxies initially available to interact.

The constancy of the brightest center galaxy luminosity was thought to be the result of homologous growth of the center galaxy, i.e. the galaxy maintains the same shape with rescaled radius and mass. Within a fixed aperture the luminosity could stay constant with growth if the surface brightness of the galaxy decreased as its scale size grew. The multiple-nuclei were viewed as the stripped cores of cluster galaxies, drifting about within the halo of the cD. Sandage & Hardy (1973) found an anti-correlation between the luminosity of the second brightest galaxy in a cluster and the luminosity of the brightest. This was taken as evidence that there were brighter galaxies in the cluster that had merged to form the cD, and the present second brightest galaxy was originally lower ranked. The current observational evidence shows no indication that the surface brightness decreases with size, however. Schneider et al. (1983) and Schombert (1984) find no anti-correlation between first

and second brightest galaxy in the cluster.

Tonry (1986) observed a distance-limited sample of multiple nuclei from Hoessel & Schneider (1985) and concludes that 65% of the nuclei have velocities in excess of 300 km/s with respect to their central galaxies. Consequently only 1/3 of sample nuclei could be interacting with the main galaxy. This indicates that many of these nuclei are not in the process of merging but instead are on radial orbits passing through the center of the cluster; i.e. they have velocities too large for circular orbits expected by dynamical friction. Since the central dominant galaxies do have normal M/L and there is no evidence for the "black pits", eccentric orbits are needed to explain the high velocities.

Also, Merritt (1984b) demonstrates that the observed properties in multiple nuclei systems can be predicted with models in which dynamical friction causes galaxy orbits to decay. This evolution can produce a substantial increase in the number of galaxies which pass near the center of the cluster without substantially lowering their mean orbital velocity. Thus the multiple systems produced would be transient phenomena having lifetimes  $\sim 10^7$  yr. The distribution of galaxy orbits ensures that an incoming nucleus would replace an outgoing one on a short timescale.

Cowie & Hu (1986) observed the faint galaxies surrounding a sample of cDs, and found that many of these galaxies were bound to the center of the cluster. These galaxies may either be infalling to the cD, or they may be of such a low mass that they are unaffected by dynamical friction. However, the dataset on which Cowie & Hu based their conclusions is very inhomogenous as the spectra of galaxies were obtained serendipitously during a study of optical filaments in X-ray clusters. Bower et al. (1988) have attempted to confirm these results with a deep sample

about the cD in A2029. They find no difference in the velocity dispersion of the galaxies close to the cD and those drawn from the general cluster suggesting that the fraction of galaxies bound to the cD is small. Unfortunately, this conclusion is weakened by the presence of unexpected structure in the velocity field which may imply severe contamination of the inner sample by a sub-clump, or that the core has not yet reached dynamical equilibrium. A detailed velocity investigation of three cD clusters by Bothun & Schombert (1988) reveals that one cluster, A2589, has a bound population with an inferred merger timescale of 3-4 Gyr. Gebhardt & Beers (1991) investigated the existence of a population of galaxies with low velocity dispersion in cores of rich clusters with a new statistical test. They claim that there is no strong kinematical evidence for the existence of low dispersion "bound" populations in the vicinity of the D/cD galaxy for most clusters. Recent velocity studies of multiple nuclei (Merrifield & Kent 1991, Blakeslee & Tonry 1992) suggest that at most 15% of these multiple nuclei are bound. A morphological analysis of multiple nuclei central dominant galaxies by Lauer (1988) shows that 50% of the nuclei display morphological disturbances such as isophotal distortions, truncated brightness profiles, and faint plumes. Many of these disturbances are explained by high velocity encounters.

The LF for cluster galaxies does not differ significantly from the field (Schechter 1976, Tammann et al. 1979). However in many cases, the cD is much too luminous to be a continuation of the cluster LF. Abell (1962) showed that there is remarkably little variation of the shape of the LF and  $L_*$  from cluster to cluster, consistent with a "universal" function that he characterizes with two power laws. This means that the processes that determined the luminosities of galaxies were either very insensitive to local conditions such as density, temperature, and turbulence/angular momentum

or that these conditions varied little from protocluster to protofield regions of space. It also implies that the evolution of the distribution of luminosities has not been substantial. Nevertheless merging, tidal stripping, and accretion are expected to produce some evolution of the LF. The LF bright end is usually very steep in clusters that have a luminous cD galaxy, i.e. there are few other bright galaxies. This again could be interpreted as the result of dynamical evolution, where the brightest have all merged to form the cD.

Tremaine (1989) contends that the resulting rate of accumulations of luminosity at the cluster center appears to be too slow by more than a factor of two to produce central galaxies with the luminosities observed, at least in virialized clusters seen today. Lauer (1988) estimates the luminosity acquired from mergers over the cluster lifetime to be  $\sim 2L_*$  which implies that a central galaxy with  $12L_*$  cannot be formed from merging processes alone. A related possibility is that central galaxies are formed before the cluster virializes, during the early stages of hierarchical clustering when the relative velocities of the galaxies are low enough that merging can occur in pairwise galaxy encounters. However, so far there are no convincing numerical models of hierarchical clustering in which the most massive stellar systems formed resemble observed central galaxies.

A survey of cD galaxies in poor clusters was completed by Thuan & Romanishin (1981). They found that the BCMs in poor clusters are missing the extended envelopes despite their apparent cD-ness, but tend to be brighter and more diffuse than giant ellipticals in rich clusters. They suggest that the lack of envelopes in poor clusters implies that envelopes in rich clusters are a result of stripped matter falling onto the centrally located cD. On the other hand, the merger rate of galaxies in poor clusters should be higher than the rate in rich clusters because of the lower

velocity dispersions. A higher merger rate could also be a reason why poor cluster cDs are more diffuse than typical giant ellipticals.

The cD envelope or diffuse light is thought to consist of either stars, unresolved galaxies, or outer halos of resolved galaxies. There are two problems with the common assumption that diffuse light consists of stars stripped from galaxies by repeated close encounters with each other (Merritt 1984a). First a large fraction ( $\sim 1/3$ ) of the cluster light is diffuse. This is equal to the luminosity contained in all galaxies greater than the characteristic luminosity  $L_*$ . Collision stripping is not that effective, and collisions cease to be important even before galaxies have lost all their dark halos. Secondly, the observed radial profile of the diffuse light is too large. Matter stripped should move into orbits nearly coincident with those of their parent galaxies. This implies that the density profile should be more centrally concentrated than that of the galaxies since the stripping timescale is a strong function of local galaxy density. Very few collisions are going on far from the center. If the diffuse light originated from galaxies, it was removed on a short timescale during the cluster collapse. Any diffuse light component present would attain the same phase space distribution as the galaxies which are undergoing violent relaxation at the same time and remain approximately unchanged as the cluster potential relaxed. Merritt contends that tidal stresses are more efficient than collisions at removing matter, and stresses are probably greatest at collapse.

In order for any of these theories to be correct the cD galaxy must not only be located at the center of the cluster but it must be at rest with respect to the cluster; otherwise, it would not remain in the center. The initial observational results seemed to confirm the cD galaxies special place. Quintana & Lawrie (1982) examined the velocities of nine clusters and their cDs. They found that the cDs are

in the kinematic center of their cluster within the errors of the velocity measurements. However, the errors were large partially due to the small number of galaxies used to determine of the cluster mean velocity. More recent studies suggest that all cDs may not be at rest at the center of their cluster. Kinematic studies of clusters of galaxies have shown that cDs often have peculiar velocities of several hundred kilometers/second (Hill et al. 1988, Sharples et al. 1988). Closer examination of the X-ray data shows that the peak of the X-ray emission may coincide with the cD but the outer isophotes are not centered on the cD (Malumuth et al. 1989). Some clusters show evidence for subsystems of galaxies which are not in virial equilibrium with the rest of the galaxies (Fitchett 1988, Bower et al. 1988). Observations of multiple nuclei BCMs suggest that cDs may be evolving but not forming in the present clusters (Lauer 1988, 1990). Several authors have suggested that cD galaxies are formed by mergers of smaller subsystems or a small subsystem with a larger cluster (Merritt 1985, Fitchett 1988, Hill et al. 1988, Sharples et al. 1988). In this case, the cDs' large peculiar velocity may be due not only to the uncertainty in determining the cluster's mean velocity but also to its recent introduction into the cluster environment. The dynamical friction may not have had time to drag the cD to the bottom of the potential well yet. Malumuth (1992), in order to test whether cD galaxies with large peculiar velocities could be formed in clusters via mergers, modified his original code, which takes into account two-body relaxation, dynamical friction, galaxy-galaxy stripping collisions, and mergers, to follow galaxy orbits in an N-body fashion. At the time of their formation the cDs have a distribution of peculiar velocities similar to that of observed cDs. However, by the end of the simulation or  $10^{10}$  yrs, the cDs have been dragged to the center by dynamical friction, and the distribution of peculiar velocities is inconsistent with what is observed. Their typical cD having nine mergers acquires a luminosity of  $5L_*$ , which

compares to Morgan poor clusters with observed luminosity of  $7L_*$ .

The cD not being at rest with respect to the cluster poses another interesting problem concerning its envelope. Either the envelope is attached to the cD and is moving with it, or the envelope is separate from the cD and the cD is moving through it. If the envelope were moving and had traversed more than roughly a tidal radius, Merritt's tidal truncation scenario suggests that the envelope would be ripped apart. If the cD were moving through the envelope, massive wakes due to dynamical friction should be visible.

### **1.3.2 Color, Velocity Dispersion, and CD Formation**

There is a well established relationship between integrated luminosity of early-type galaxies and their color such that more luminous galaxies are redder (Sandage & Visvanathan 1978). Similarly, concentric aperture photometry showed that galaxies are redder at smaller radii (Sandage 1972, Persson et al. 1979). These two phenomena are thought to have common physical origin: higher metallicity of the stellar population in more luminous galaxies and in the centers of individual galaxies. Hausmann & Ostriker (1978) suggested that the galactic environment may produce systematic deviations from the mean color-magnitude relation. Their cannibalistic model predicts first-ranked galaxies in early Bautz-Morgan type clusters should be at least 0.1 mag bluer in U-B than their counterparts of the same magnitude in later-type clusters. In their model, cDs are the result of galaxy accretion. Thus the color of the cD will eventually be dominated by the smaller bluer galaxies it devours. The 0.1 mag increase is an order of magnitude estimate as this model is based on a number of simplifying assumptions, such as quasi-homologous growth, no galaxy color gradients, and mass, energy, and luminosity conservation at coalescence. Lugger's (1984) observations rule out a color difference as large as 0.1 mag



in U-B between cD and normal first ranked galaxies to the  $5\sigma$  level.

Models of formation of galaxies involving the isolated collapse of a protogalactic gas cloud have been shown to generate color gradients. Continuous color gradients from nucleus to halo are thus considered evidence for galaxy formation via dissipational processes. Larson's (1975) models are now known to rotate too rapidly and have isochromes too flat compared to observation. Larson derives extreme (10:1) flattening of isochromes due to angular momentum. However, these models may not be consistent with results which suggest that giant ellipticals are flattened by anisotropic velocity dispersions. Carlberg (1984) did N-body simulations of the isolated collapse of a gas cloud and included the effect of star formation sites. His models rotate more slowly, have less flattening of isochromes, and predict more luminous galaxies have steeper gradients. Models treating collapse as dissipationless (Gott & Thuan 1976, van Albada 1982) predict an accumulation of gas confined to the inner regions, limiting the radius over which the color gradient could exist.

Up to now most studies have shown cDs to have small or flat color gradients. The minimal nuclear color gradients support the scenario in which mergers diminish or wash-out pre-existing gradients. White (1980) predicts a drop in the gradient by  $\sim 20\%$  for one merger event and  $\sim 50\%$  from three binary mergers; however, star formation triggered by these events was not taken into account. Red envelopes (or a lack of blue envelopes) may imply that the source of the stripped material is red galaxies rather than spirals. This is plausible because cDs are only associated with high density regions and these regions are rich in early-type galaxies. The lack of blue envelope colors also contradicts the expectations of cooling flow scenarios which produce recent epoch star formation. Fabian et al. (1984) ran simulations that produced red, low mass stars from cooling flows and colors similar to those

found in giant ellipticals. However, these processes should be confined to the cores of BCMs where the gas densities are high enough for star formation, which seems unlikely in the extended envelopes. Sarazin's (1988) metallicity estimates of the hot intra-cluster gas range from 0.5 to 1.0 solar suggesting that the cluster gas is not abundant enough to produce a metal-rich stellar population in the envelope. Another possibility is that there exists a population of asymptotic giant branch stars which are luminous, evolve rapidly, and dramatically influence red and infrared colors (Chokshi & Wright 1987). Such short-lived populations may be present after periods of high dynamical activity (stripping and merging). On the other hand, the dust content in clusters is still up for debate. Hu (1992) derives an average excess reddening of  $E_{B-V} \sim 0.19$  above the foreground extinction for 10 cooling flow clusters. Hu contends the majority of the reddening may be associated with the extended cluster component.

Rising velocity dispersions profiles have not been seen in normal elliptical galaxies. In most cases their dispersions fall with radius, although there are some that apparently remain flat. The velocity dispersion of the cD in evolutionary schemes that rely on tidal stripping and mergers to form the cD/envelope should be representative of the high-velocity dispersion,  $\sim 1000$  km/s, of the cluster members. The results of Dressler's (1979) study confirm an increase in velocity dispersion from roughly 300 to 500 km/s which is a necessary but not sufficient condition for the stripped debris hypothesis. It has been suggested that the difference in the velocity dispersion of the nucleus and cluster indicates a different origin for the stripped material comprising the cD and envelope. The fact that the stars are bound to the system with this high velocity dispersion implies that the M/L increases significantly. The fate of these halos is quite different than those of galaxies in the field. For

although field galaxies should be able to hold onto their extensions, cluster galaxies should be stripped, thus making that material the common property of the cluster.

The velocity dispersion increase can be interpreted as evidence for a component of high  $M/L$  with a more extended mass distribution than that of the luminous matter. Dressler (1979) fashioned a model which accounted for all observed properties of A2029 including the luminosity profile of the cD, its dynamical structure, the high velocity dispersion, and apparent mass discrepancy. A three-component King model composed of a normal elliptical galaxy, a high  $M/L$  cluster-filling and -binding superstructure, and a component of intermediate  $M/L$  and velocity dispersion which supplies the light of the extended halo. The high  $M/L$  component is tentatively identified with stripped dark halos of cluster galaxies, and the intermediate  $M/L$  material is attributed to the dynamical friction process which disrupts massive luminous galaxies as they encounter the cD envelope. Alternatively, Tonry (1983) has suggested that these observations may be compatible with models in which the  $M/L$  is assumed to be independent of radius. The rise in the velocity dispersion with radius is then explained by invoking highly anisotropic velocity dispersions such that the motions of stars in the halo are almost entirely tangential. Carter et al. (1985) data cannot distinguish unambiguously between isotropic models with dark matter and constant  $M/L$  models with large negative anisotropy. The first model has isotropic velocity dispersions and a two component mass distribution: a bright component with a King density distribution and a dark, isothermal component with a density distribution which is slightly more concentrated than that of the galaxies. The second model has predominantly tangential motions in the galaxy halo and no dark component. As is the case for most bright ellipticals, supergiant galaxies are not flattened by rotation. Rotation is more important in faint ellipticals (Davies et

al. 1983).

In support of a primordial origin of a non-extensive envelope are studies that show cDs flattened and aligned to the overall distribution of cluster members on scales up to 15/h Mpc (e.g. Sastry 1968, Carter & Metcalfe 1980, Binggeli 1982, Struble & Peebles 1985, Rhee & Katgert 1987, Lambas et al. 1988). Similarly, Struble (1987) has analyzed the distribution of 21 central dominant galaxies and has found that both bright and faint isophotes are aligned with the cluster major axis. There is also a tendency for the cD to be aligned with the nearest neighbor cluster on scales less than 15/h Mpc.

Rhee & Roos (1990) investigate this alignment property by addressing the following question: under what conditions will the initial large-scale anisotropy be communicated to the innermost regions of the collapsed and virialized systems ? They find that during the collapse of prolate, initially homogeneous ellipsoids, information concerning the orientation is transmitted to the center of the particle distribution. The way this is transferred is determined by the processes which occur during violent relaxation. Rhee & Roos find that cDs show a similar increase in ellipticities of isophotes from the center as found in first-ranked galaxies in a manner that indicates that they are predominantly prolate (Porter 1988). Their results suggest that first-ranked galaxies are formed during the collapse of the cluster as a whole and that they are generally, but not always, at rest at the cluster center. The authors also note that their results do not depend sensitively on the amount of substructure that exists during the collapse.

#### 1.4 Previous Diffuse Light Measurements

A low surface brightness or diffuse component of the cluster light has been

measured in several D and cD clusters. The most relevant measurements for this investigation are Oemler (1973) for A2670 and Uson et al. (1991; hereafter UBK) for A2029.

The earliest investigations to determine the fraction of diffuse light in clusters yielded generally inconclusive results. De Vaucouleurs & de Vaucouleurs (1970) estimated that in the Coma cluster, 40% of the light due to galaxies brighter than 19th magnitude is from intergalactic matter, but concluded that most or all of this is due to the faint outer parts of the brightest cluster galaxies. Baum (1973) photoelectrically intercompared the surface brightness of several vacant patches in the fields of A1132 and A801 and found the excess light to be about 17% of the galaxy light contained within a non-redshifted isophote of 26th magnitude. All of this light could be accounted for by dwarf galaxies below the detection threshold and the overlapping outer parts of bright galaxies. Similar conclusions for Coma were reached by Melnick et al. (1977) with photoelectric drift scans and a sky monitor telescope. They found an upper limit of 25% of the total cluster luminosity comes from the intra-cluster medium (ICM). From an analysis of the isophotal contours on the Palomar plates, Thuan & Kormendy (1977) found a value of 31% for the diffuse component in Coma. Oemler (1973) measured the surface brightness profile of A2670 using a method of isophotometry on green photographic plates. He reports that the cD has the structure of an elliptical galaxy out to 30 kpc and with an enormous envelope traceable out to 1 Mpc which contains 35% of the cluster light. Gudehus (1989) reports little if any diffuse light exists on the spatial scale equal to that of the cD cluster in A1689 using a new method of surface photometry applied to CCD exposures. He considers the diffuse light to be separate from the cD and attempts to measure it after the cD profile has been subtracted. Malumuth &

Richstone (1984), making use of the photometry of Malumuth & Kirshner (1981), claim up to 60% diffuse light for richness class 3 clusters, with richer clusters having more light. Their results also agree with computer simulations of tidal stripping. There is some concern that their definition of excess light (as compared to a King model) biases their estimates upward.

The results of the following investigators are discussed in more detail elsewhere in this manuscript. In an effort to study color and the stellar content of cD galaxies, Mackie et al. (1990) and Mackie (1992) did surface photometry of the innermost regions of several D and cD galaxies. Schombert (1988) did single-band photographic and CCD surface photometry to study the extended faint envelopes around 27 cD galaxies. In his study, he only considers those envelopes which show a "break" from the surface brightness profiles of the parent galaxy. UBK use a statistical method on a mosaic of CCD images to trace the surface brightness profile of A2029 out to 425/h kpc. They report that 23% of the total cluster light is emitted by the cD/envelope.

## 1.5 This Investigation

This investigation describes some new techniques to study diffuse light in galaxy clusters as is applied to two cD clusters A2670 (Scheick & Kuhn 1993) and A2029. The approach is to measure the large- and small-scale anisotropy of the diffuse light in order to address some questions concerning the origins of the diffuse light and general cluster evolution.

In the case of A2029, the UBK measurement shows the extended halo following a de Vaucouleurs' profile very closely out to 425/h kpc. The smoothness of this halo, as well as that for A2670 implies that the ICM is well-homogenized, which is

surprising in light of the violent galactic interactions that are thought to be presently occurring in the cluster. Thus we are motivated to determine just how smooth the profile is. With deep CCD images, we measure the fluctuations or small-scale structure in the diffuse light. The structures that we might expect are clumpiness from galactic stripping mechanisms of whose shape we do not have apriori knowledge, or possibly over-densities or wakes as evidence of galactic passage, on the spatial distribution of which there has been much theoretical work done (Weinberg 1989, Mulder 1983). Most studies on clusters of galaxies attempt to map the cluster potential using the distribution of the galaxies themselves, or of the X-ray emitting gas, which could in principle place strong constraints on the mass distribution (and dark matter). We can turn the tables on this problem if we use the diffuse light photons as the test particles, which have the obvious advantage over using galaxies or X-rays in sheer number, and better “counting” statistics. From this approach, we can ask direct questions of the cluster concerning the source of the diffuse light.

A2670 is the nearest ( $z \sim 0.076$ ) Abell cluster of richness class 3 with a supergiant cD. Sharples et al. (1988) measured velocities for 220 cluster members and obtained a cluster mean velocity of  $22,843 \pm 64$  km/sec and a cD velocity of  $23,282 \pm 100$  km/sec. They concluded that the hypothesis that the cD lies at the dynamical center of the cluster can be rejected at more than the 99.9% confidence level. There is no evidence for significant subclustering in A2670 (although see Bird 1993 for an alternative analysis of the Sharples et al. data). It is not a particularly strong X-ray source ( $L_x \sim 10^{44}$  ergs/sec, Jones & Forman 1984); a radial X-ray profile is shown in Sharples et al. (1988).

A2029 has been extensively studied (see Dressler 1981 and references therein; see also Malumuth & Krishner 1985, Schombert 1987). Dressler’s estimate of the

LF shows the cluster to be one of the richest clusters in the sky with an estimated richness 4.4 on Abell's scale. It has a redshift of 0.0767. Its velocity dispersion is  $1450(+185,-140)$  km/s determined from 47 galaxies (Bower et al. 1988). The cluster is also a copious emitter of X-rays (McHardy 1978). Sarazin et al. (1992) report X-ray emitting filaments from ROSAT images of the cD. There is some evidence that indicates either the cluster center is contaminated by a foreground subclump or the core is not in virial equilibrium (Bower et al. 1988).

The remainder of this thesis is outlined as follows: Chapter 2 describes the data, and chapter 3 describes a multi-faceted analysis of these data. Chapter 4 provides a discussion as to how these results compare to previous measurements and what they tell us about cluster evolution.



## CHAPTER 2

# OBSERVATIONS AND DATA REDUCTION

### 2.1 Observations

#### 2.1.1 A2670

We observed Abell 2670 with the 0.9m telescope at Kitt Peak National Observatory (KPNO) on September 4-9, 1991. We used the NOAO ST1K direct CCD chip which has a relatively high full well capacity ( $4.0 \times 10^5 \text{ e}^-$ ) and quantum efficiency (66.3% at 700nm). The detector was mounted at the f7.5 Cassegrain focus. The pixels are  $0.59''$ , adequate to the marginal seeing conditions of about  $2.10''$  (full width half maximum, FWHM, of the stellar radial profile). We used Harris R and V filters.

The 3 tessellated frames analyzed in this thesis were produced from data taken over 3 separate nights. The exposure times were limited to 900 s to avoid over saturating the stars in the field. The pattern of observations of the cluster was first a center frame, then four frames offset  $3'$  in each direction, a center frame, four frames offset  $5'$ , and then repeat the whole sequence. On the most productive nights, we obtained several hours integration time on the cluster center. However after processing, we found that only 12 R frames (3 hours total) on the 3rd night, 6 V frames on the fourth night, and 5 R on the fifth night were useful for this analysis. We also made observations of fields approximately  $30'$  north and south of cluster center, as representative of the background.

We observed a set of standard stars from Landolt's UBVRI secondary calibration list (Landolt 1983). The secant law corrections were as large as 0.1 R magnitudes, while repeatability of our standard star observations was approximately 0.05 R magnitudes. The light scattering properties of the telescope and detector optics were measured with observations of the bright star Altair during 1 s exposures. The point spread function (PSF) was constructed by matching the wings of Altair to the profile of an appropriately scaled bright Landolt star in our calibration frames. Dark frames for all data frame exposure lengths were taken, as well as the standard out-of-focus exposures of a white spot on the dome to produce domeflats, which were used only in zeroth order processing.

### 2.1.2 A2029

We observed Abell 2029 on the KPNO 2.1m telescope on June 4-8, 1992. We used the TIKA CCD chip which is characterized by a linearity limit of  $2.5 \times 10^5 \text{ e}^-$  and good quantum efficiency (82% at 700nm). The CCD camera was mounted at the RC focal plane (f7.5). The pixels are 0.267" on a side. The seeing conditions were roughly 1.5" over the observing run. We again used a Harris R filter.

The two tessellated frames analyzed here were produced from data taken on two separate nights. The exposure times were 120 or 600 s on the two different nights. With the shorter exposures, we were only using our observing time with 50% efficiency. We opted to increase the exposure time to 600 s regardless of saturating the brighter galaxies in the frame. As we are interested in obtaining the deepest exposure of the cluster center, we took observations offset anywhere from 5" to 90" from the center in one of the four directions. After processing, we found 35 R frames (120 s exposures) on the first night and 23 R frames (600 s exposures) on the third night were useful for this analysis.

We again observed a set of standard stars from Landolt’s UBVRI secondary calibration list. Unfortunately, our 5 s exposures saturated all standard stars making them useless for calibration purposes. This was not a problem as we were not interested in correcting the diffuse light profile for scattered light and could calibrate with previous measurements of the diffuse light profile. Again, dark frames for all data frame exposure lengths and dome flats were taken.

## 2.2 Data Reduction

### 2.2.1 Standard Processing

For the A2670 data, the images were first corrected for dark current by subtracting an average dark frame of the appropriate exposure length. Calibration of the pixel-to-pixel gain variations was accomplished by producing a median flat with 8-16 frames from each night’s data. We can estimate how well we are flat-fielding by computing the root-mean-square (RMS) variation per pixel in an image of the ratio of two R flats. The variation is 1.8 %, which is slightly less than the per pixel shot noise we expected. The mean sky brightness was roughly 22.3 R mag/arcsec<sup>2</sup>.

For the A2029 data, we relied on an algorithm developed for calibrating the spatial nonuniformity of the CCD array (Kuhn et al. 1991). This technique uses the information in multiple, spatially displaced data images to determine the pixel gain variations, even when the sources are extended. Input to this algorithm were 16 cluster data frames that had been dark subtracted, flattened with a dome flat, and scaled to have the same mean intensities. After 20 iterations, a flatfield was produced. The integrity of this flatfield was checked by comparing it to one produced from a different subset of cluster data frames. The RMS variation per pixel of an image of the ratio of two flats is 0.4%, which is on the order of the per pixel shotnoise

expected if the sky brightness is roughly 60% of the full well capacity of the CCD (we do not have a measure of the mean sky brightness due to the lack of calibration stars) . It should be noted that the algorithm failed to produce a flat for 13 frames taken during the second night as there was as much as 0.2 mag difference in the brightness of several galaxies over the course of the night due to high cirrus clouds. Data from this night was not used in the analysis.

### 2.2.2 Shifting and Tesselating

As we are interested in measuring small-scale structure in the cD envelope, we need the deepest observations possible. In order to do this with our exposure time per image, we must first shift the images to common coordinates and then tessellate them. Sensitivity of our measurements to the inhomogeneity in the diffuse light, be it wakes or other structure, requires that we determine the image shifts to sub-pixel accuracy in order not to degrade our resolution. We devised a method which uses information at all frequencies (instead of interpolation methods which smooth out higher frequencies) to determine the fractional shift.

Letting  $D_r(\mathbf{x})$  be the reference frame data,  $D_s(\mathbf{x})$  be the data of the shifted frame, and  $\delta$  be the offset of a shifted frame with respect to the reference frame, we have

$$D_s(\mathbf{x}) = D_r(\mathbf{x} + \delta)$$

If we take the Fourier transform (FT) of  $D_r$  and  $D_s$ ,

$$D'_r(\mathbf{k}) = \int D_r(\mathbf{x}) e^{i\mathbf{k} \cdot \mathbf{x}} d\mathbf{x}$$

$$D'_s(\mathbf{k}) = \int D_s(\mathbf{x}) e^{i\mathbf{k} \cdot \mathbf{x}} d\mathbf{x}$$

and then substitute the first relation for  $D_s$  into the previous equation, we get

$$D'_s(\mathbf{k}) = \int D_r(\mathbf{x} + \delta) e^{i\mathbf{k} \cdot \mathbf{x}} d\mathbf{x}$$

or with a change of integration variables to  $\mathbf{y} = \mathbf{x} + \delta$

$$D'_s(\mathbf{k}) = \int D_r(\mathbf{y}) e^{i\mathbf{k} \cdot (\mathbf{y} - \delta)} d\mathbf{y} = D'_r(\mathbf{k}) e^{-i\mathbf{k} \cdot \delta}.$$

We now minimize the following expression for  $\delta$ :

$$(\mathbf{k} \cdot \delta - i \ln[\frac{D'_s}{D'_r}])^2.$$

We can perform the shift in Fourier-space and transform the shifted image back to real-space.

To solve the equation for  $\delta$  we used an amoeba algorithm (Press et al. 1992). This algorithm implements the "downhill simplex method" for multi-dimensional minimization. A N-dimensional simplex is a geometric figure of N+1 vertices with interconnecting line segments. To use this method, an initial simplex must be defined from the starting point  $\mathbf{P}_o$ . The remaining N points are given by  $\mathbf{P}_i = \mathbf{P}_o + \lambda_i \mathbf{e}_i$  where  $\mathbf{e}_i$  are N unit vectors and  $\lambda_i$  is a guess of the problem's characteristic length. The downhill simplex method takes a series of steps, most of which entail moving the point of the simplex where the function is highest through the opposite face to a lower point, while maintaining the volume of the simplex. When it can, the method expands the simplex to take larger steps. When it reaches a "valley floor", the simplex tries to move along the valley. The simplex contracts itself in all directions if it surrounds the lowest point. The algorithm terminates when the decrease in the function value in the last step is fractionally smaller than some input tolerance level. Generally speaking, a tolerance of  $10^{-7}$  took approximately 40

iterations. The amoeba algorithm was able to reproduce a solution to the requested tolerance level from any reasonable initial simplex, though it is not by any means the fastest algorithm. It also failed to find shifts when there were large positional offsets between frames. For those images offset 3' and 5' from center, we approximated the correct shift by a whole number of pixels and then used the amoeba algorithm to find the fractional shift. All k-space does not provide useful signal. Images of  $D'_s/D'_r$  revealed a distinct plane wave pattern for  $k$  less than roughly 100. We took  $k = 128$  for all shifts. Unfortunately, the amoeba routine does not readily provide a standard error for the derived shift values. We checked its performance by mapping the solution space to see that it had reached the true minimum (instead of a local one). We also produced a histogram of the separations between the IRAF APPHOT package (Davis 1989) coordinates of objects in a reference frame and a frame that had been shifted using the Fourier algorithm. A Gaussian fit to this histogram yielded a mean of zero for the object position differences to within the IRAF object position uncertainty, lending confidence in our shift algorithm.

There is a drawback to using this method: the FT and inverse FT produce a "Gibb's ringing" at any point, line, or patch of discontinuity. Saturated stars and hot columns transform back with associated spikes (alternating bright and dark pixels) in the horizontal and vertical directions from the object. Fortunately, for our purposes, this was not a problem. For the hot columns, we substituted the image mean. The saturated stars' profiles could still be measured and removed in the PSF subtraction process. The ringing has a mean of the zero-point of the image and therefore does not contaminate our measurement of the diffuse light. Also, as we know how the ringing autocorrelates, we could distinguish it from any other signal. Finally, since the ringing is only present near the image defects and discontinuities,

it cannot be responsible for any of our results which show a dependence on distance from the cluster center.

After producing a set of shifted images per night, we averaged them per pixel. The A2029 data was particularly contaminated with cosmic ray hits; we averaged these frames robustly to remove them (i.e. computed a mean and standard deviation per pixel and then computed a mean from those pixels whose intensity values lie within the original mean  $\pm 2.5$  standard deviations). Our A2670 dataset consists of three frames: a tessellation of 12 in R, 5 in R, and 6 in V. For A2029, we have two frames: a tessellation of 21 and 35 in R, the former having roughly 1.5 the signal-to-noise (S/N) of the latter. We also note that a comparison of radial profiles of objects in a single frame and the final tessellation did not reveal any systematic degradation in the FWHM of the star-like objects.

### **2.2.3 General Photometry and PSF Subtraction**

The following discussion of photometry and PSFs concerns the A2670 dataset. The A2029 dataset was calibrated against the diffuse light measurement of UBK by matching profiles in the radial range for which the ellipticity is roughly constant and there is minimal contamination by scattered light.

Photometry was performed using IRAF's PHOT routine assuming an uncrowded field. All parameters were left at their standard defaults with the obvious exceptions of the detector characteristics, exposure time, and image dependent parameters. We used an aperture radius of 9 pixels or 5.3" (the FWHM for galaxy-like objects being  $\sim 4$ -5 pixels).

In order to measure the diffuse light profile cleanly at large radii, we must first correct for the contamination of scattered starlight by subtracting a scaled PSF

representing it. A PSF for both R and V bands was constructed using a bright Landolt standard for the inner 6' and a power law fit to the wings of Altair for larger radii. The scattered light for all objects brighter than 17 R magnitudes was removed by the scaled PSF subtraction, excluding the cD itself. The 13 saturated stars presented us a special case. As there were no magnitudes available, we relied on fitting a power law to the aureole. A survey of the surrounding Palomar plates revealed no objects bright enough to affect our field.



## CHAPTER 3

### Analysis

#### 3.1 A2670

##### 3.1.1 Diffuse Light Profile

Figure 1 is our deepest (3 hr) R-band tessellated image of the central  $10' \times 9.7'$  of A2670. The faintest objects visible in this figure are roughly  $23.9 \text{ R mag/arcsec}^2$ . Figure 2 shows a contour map of the central  $1 \text{ arcmin}^2$ . The lowest contour is 0.1 A/D units, and the contour interval is 0.7 A/D units. The tick marks in this figure denote pixels. The isophotes that characterize the halo are circular about a common center, which we take to be the spatial center of the cD. Using the statistical method to determine the diffuse light described in UBK, the diffuse light profile can be measured out to  $\sim 3.5'$  from the cluster center, at which point the diffuse light signal slips into the background noise. This method basically involves fitting truncated Gaussian distributions to the histogram of pixel intensities found within a radial bin, the distribution mean taken to be the diffuse light intensity for that bin. As shown in UBK, the subtraction of the contaminating scattered light from bright stars has a noticeable effect on the diffuse light profile.

The choice of the zero-point or background does have some effect on how far out the diffuse light can be measured. Figure 3 shows the diffuse light as a function of radius of  $1'$  to  $5'$  from the cluster center. We take the zero-point to be  $-0.00435 \pm 0.00020$ , the value at which the diffuse light signal is no longer decreas-

ing. We are confident we are measuring the true extent of the diffuse light as we find the same result from a super-tesselated frame formed with 17 individual frames from our 2 separate nights of R-band data. Thus the diffuse light extends to approximately 3.5' or 230/h kpc.

The RMS variation per pixel of the sky is about 2%. In our outermost bins, there are on the order of 5000 pixels. Hence we are measuring a diffuse light signal that is  $\sim 0.01\%$  of the sky brightness. The conversion from A/D units to mag/arcsec<sup>2</sup> is  $23.19 - 2.5\log(\text{A/D units})$ .

Figure 4 shows the best fit de Vaucouleurs' profile (dashed line) for both the R and V band data (points). This profile has the following functional form (de Vaucouleurs 1948):

$$I(r) = I_0 e^{-ar^{0.25}}$$

where  $I$  is the mean intensity in the radial bin whose central value is  $r$  and  $I_0$  and  $a$  are coefficients determined in the fitting procedure. The fit for R band has a reduced  $\chi^2$  of 0.35, while that for V has 0.28. We should note that, although not shown, the de Vaucouleurs' profile fits poorly within a radius  $\leq 8''$  of the center; this is also true of a King profile and a power law.

What percentage of the total cluster light is the diffuse light ? Figure 5 shows a log-log plot of the total R-band cluster light (solid line) and the diffuse light (dashed line) versus radius. The total light follows a power law for all radii. For smaller radii, the diffuse light follows the total light, as expected, considering the sparsity of objects in this region, but falls away for radii greater than roughly 1'. We measure the total cluster light up to each radius in two ways: (i) simply integrating the counts per radial bin directly from the image, (ii) integrating the

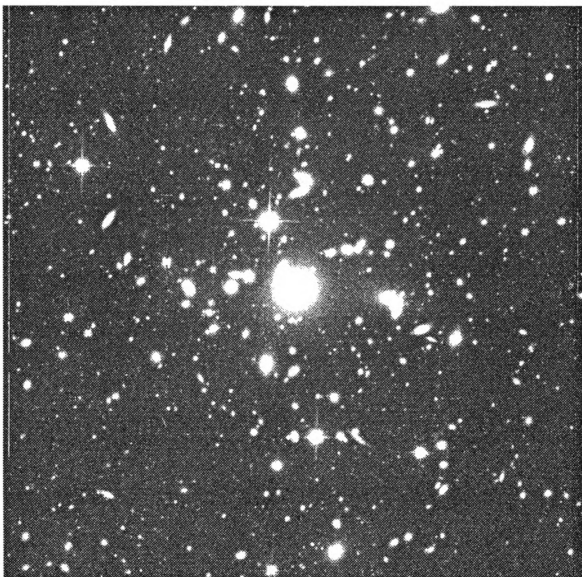


Figure 1: Gray-Scale Image of the Central 10 arcmin<sup>2</sup> of A2670.

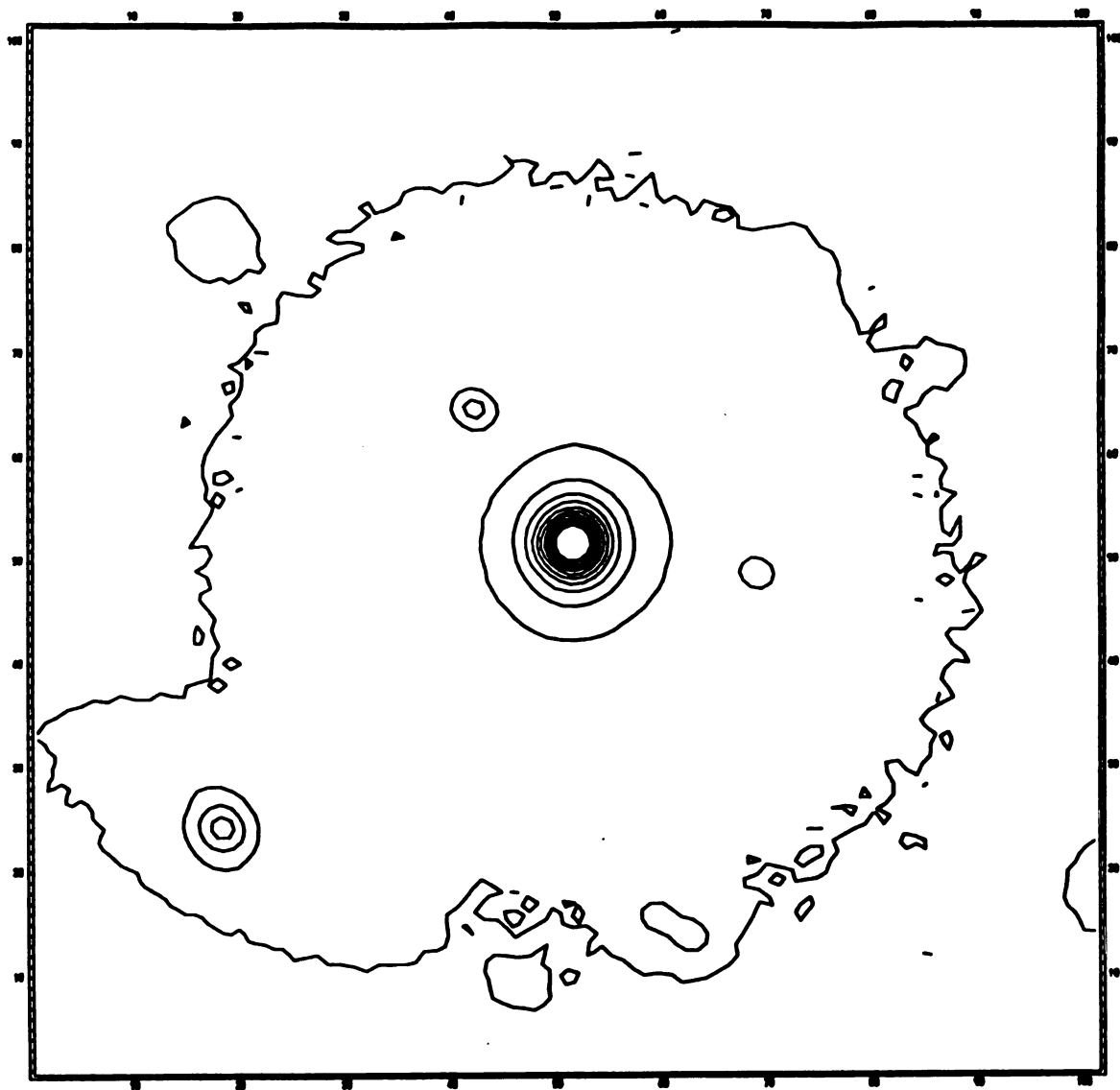


Figure 2: Contour Map of the Inner 1 arcmin<sup>2</sup> of A2670.

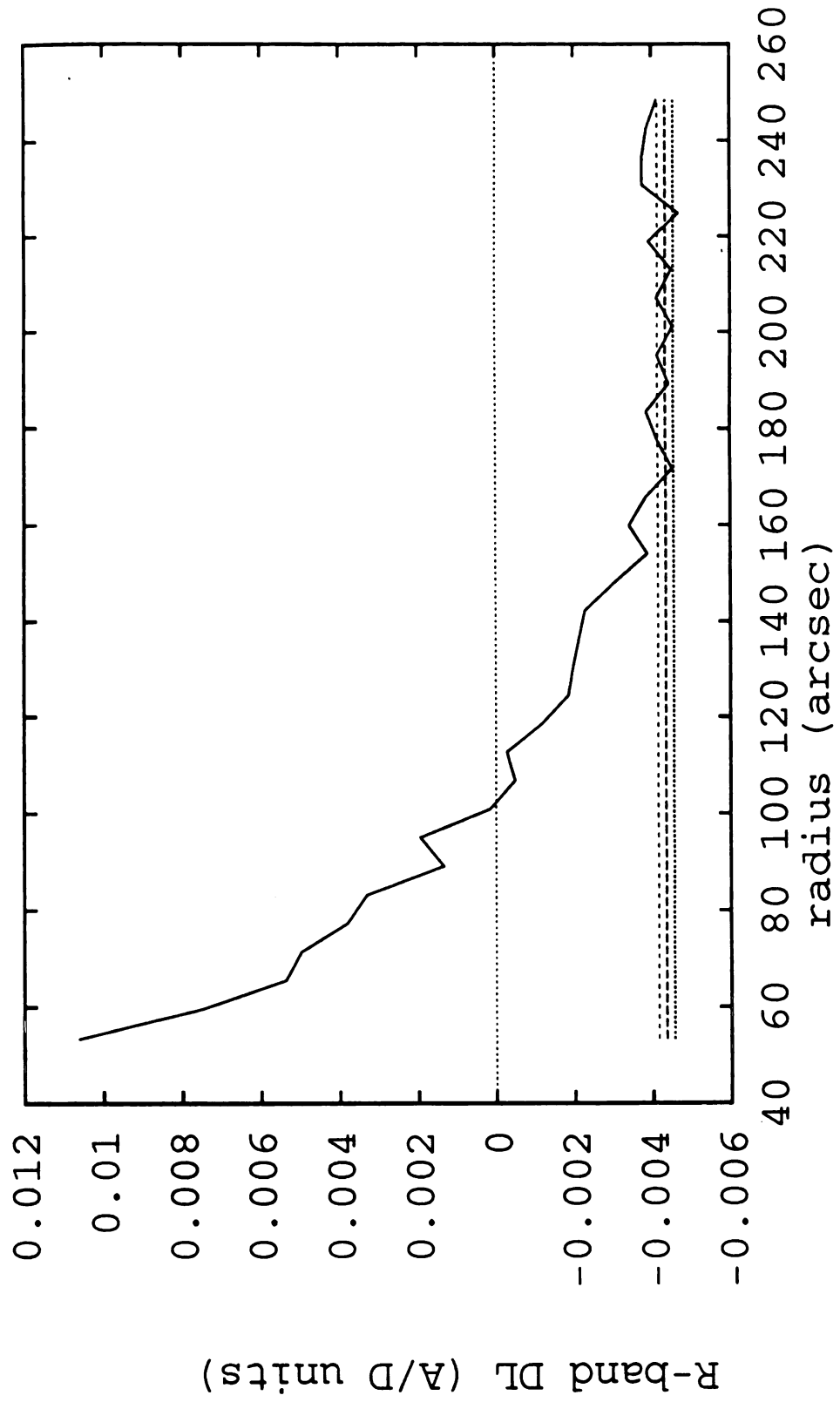


Figure 3: Outer R-band Diffuse Light Profile in A2670.

counts per radial bin converted from IRAF PHOT detected objects plus the diffuse light profile. We cannot directly remove the background galaxies as we do not have precise differential photometry that is accurate from the cluster center out to the “background” (a few degrees from cluster center). In addition, our offset frames (30' from the cluster center) have a different object detection threshold. Without this correction, the integrated total cluster light rises faster than the expected function. We can estimate effects of our background uncertainty on the ratio by subtracting a constant which forces the cluster light to go to zero for the outer 1' of our image. We note that the core radius as calculated by Dressler (1978b) is 0.31 Mpc for an  $H_0 = 50$  km/s/Mpc (or 160/h kpc in our notation), implying that the outer region considered could be only 3-4 core radii away, though this number may not be relevant in this context as it is the point that the number density falls to half of its central value, not the light distribution. The ratio of the diffuse light to the total cluster light at a radius of  $\sim 3.5'$  is roughly 0.30 when integrating total light from the image directly, and roughly 0.37 when using the photometry list to compute the contribution of the flux per object to the total cluster light. Assuming a zero background, the ratio is 0.29. The correct background is somewhere between these numbers such that we can use their difference (0.08) as an estimate of the systematic uncertainty in our measurement.

The remainder of the analyses was done using the residual image produced by subtracting the diffuse light profile. This was done in two ways: (i) subtracting the actual statistical determination of the diffuse light per radial bin, (ii) subtracting the de Vaucouleurs' profile fit to that determination. The former is rougher within a radius of 30" as the radial bin width has to increase to maintain a statistically significant number of pixels per bin. No diffuse light measurements were taken

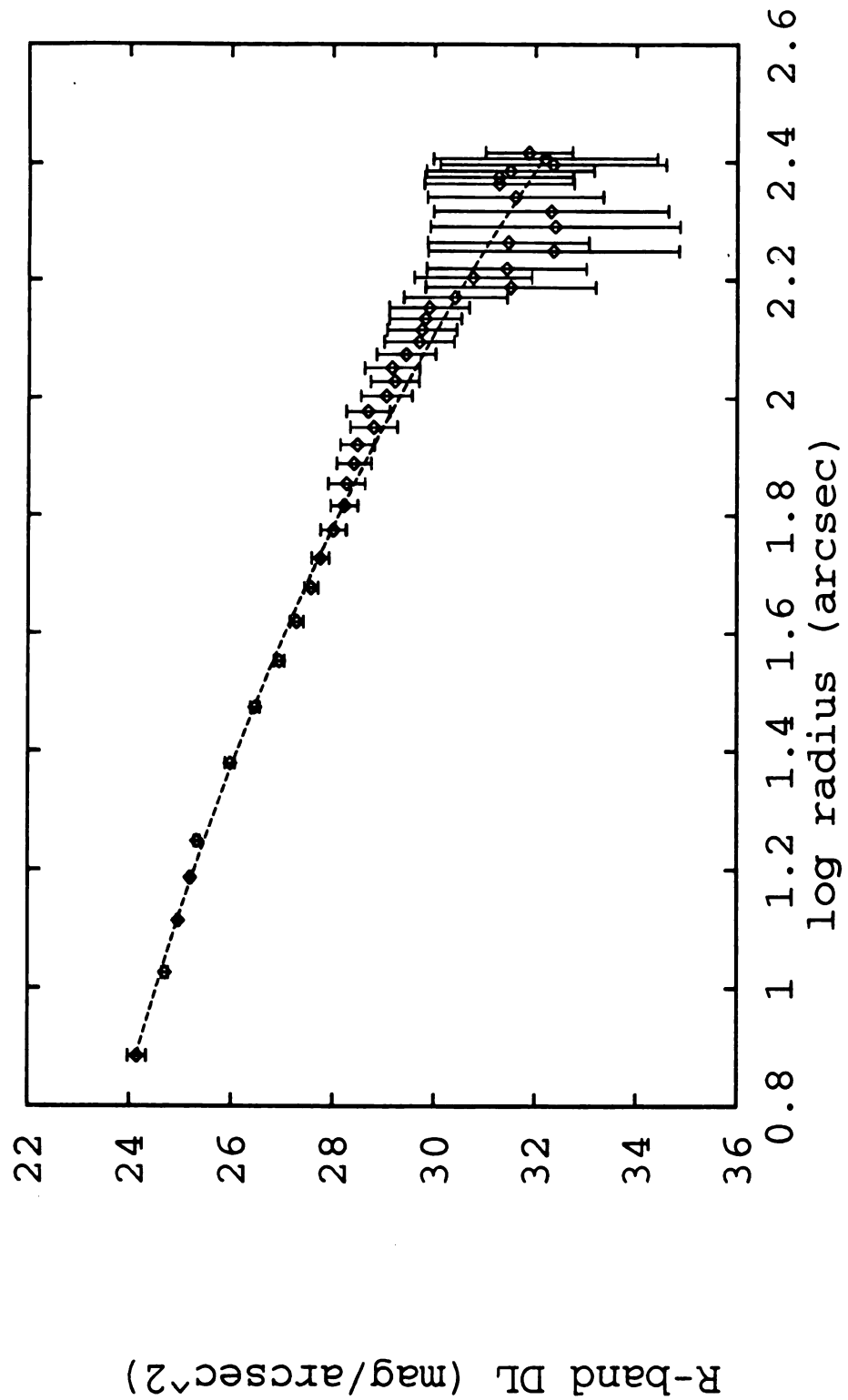
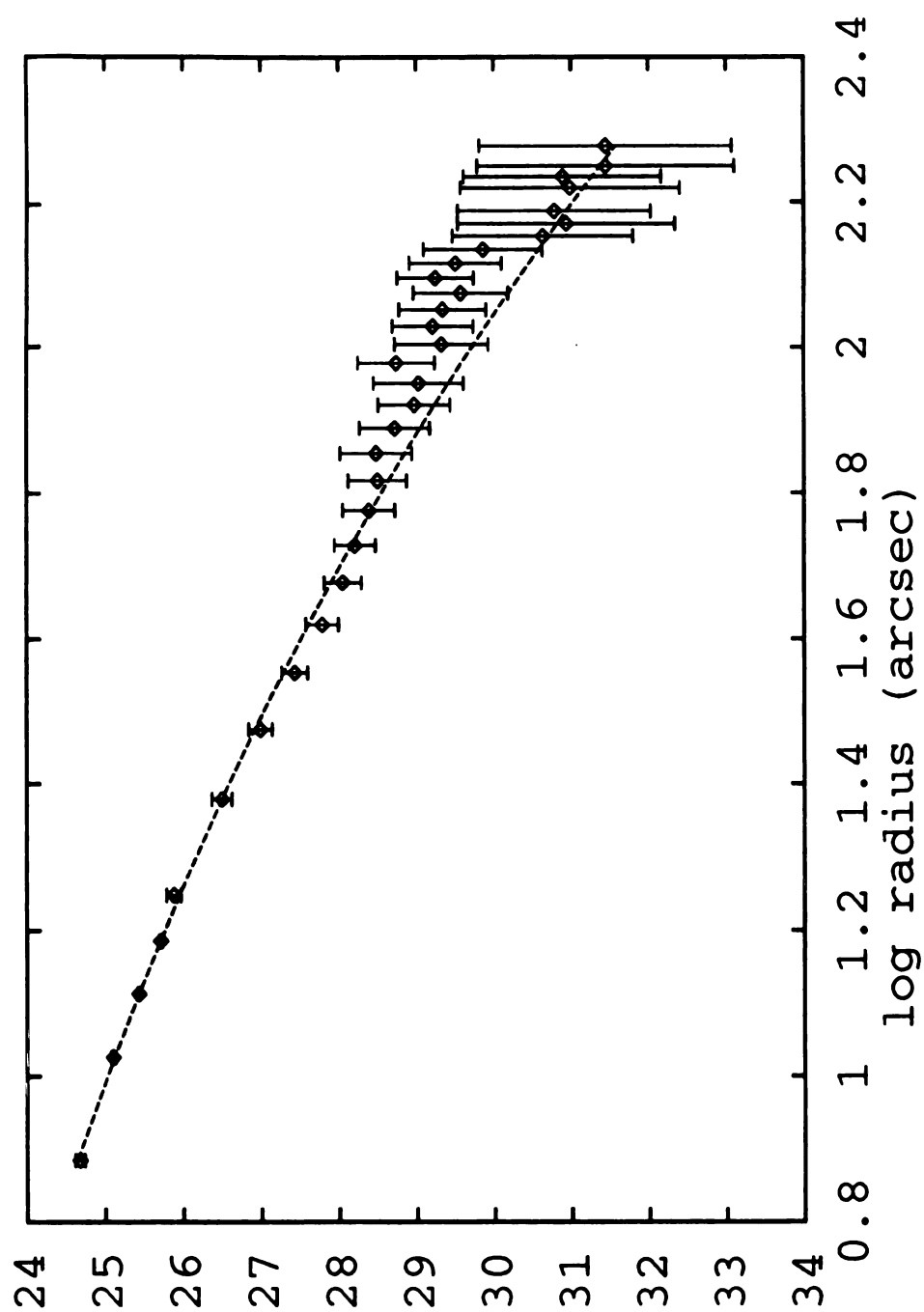


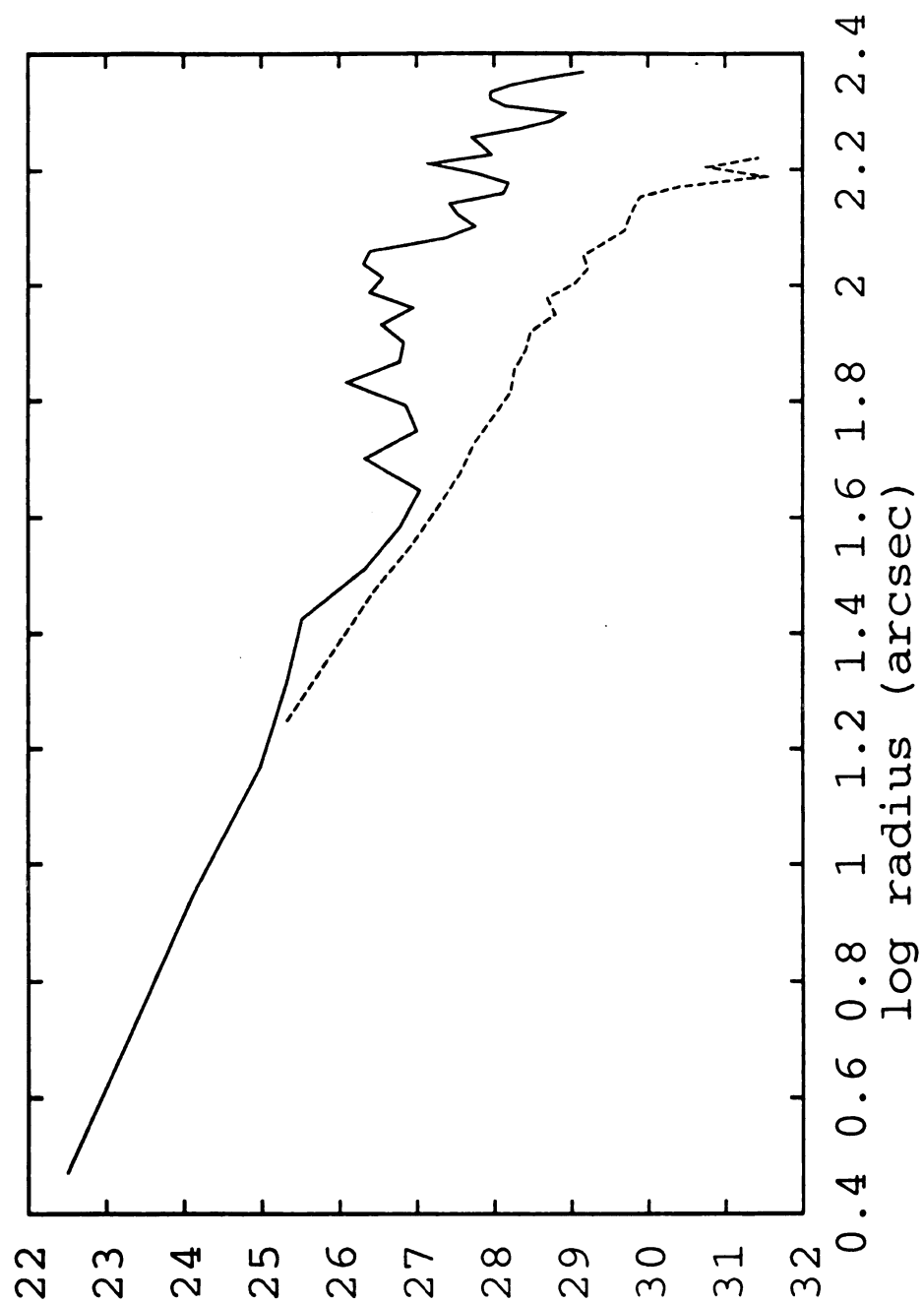
Figure 4a: De Vaucouleurs' fit to R-band Diffuse Light Profile in A2670.



V-band DL (mag/arcsec<sup>2</sup>)

Figure 4b: De Vaucouleurs' fit to V-band Diffuse Light Profile in A2670.





DL & CL (mag/arcsec<sup>2</sup>)

Figure 5: Total R-band Cluster Light & Diffuse Light in A2670.

within 8" due to the minimal number of pixels and the poor de Vaucouleurs' fit in that region.

We used our measurements of the surface brightness fluctuations to place limits on the number and luminosity of objects that contribute to the diffuse light in each pixel (analogous to Tonry & Schneider's 1988 approach to measuring the distance to galaxies from surface brightness measurements). Since our pixels may be smaller than a typical contributing galaxy from the faint unresolved end of the galaxy LF, we first rebinned the data to a 2x2 pixel scale. If we now characterize the luminosity of a faint contributor by  $l_o$ , and if there are on average  $n(r)$  objects which contribute to a pixel at a given projected radius  $r$  from the cluster center, then we expect a mean surface brightness profile of

$$S(r) = \frac{l_o n(r)}{4\pi d^2}$$

for a cluster at distance  $d$ . The variance in the surface brightness in a ring of pixels at distance  $r$  from the cluster center should be

$$\sigma^2(r) = \frac{l_o^2 n(r)}{(4\pi d^2)^2} + \sigma_o^2$$

as long as each pixel samples an independent line of sight, and where other sources of measurement noise are contained in the  $\sigma_o^2$  term. Since the sky background in our data is much larger than the diffuse light signal, both photon and CCD read noise contributions to  $\sigma(r)$  should be independent of the distance to the cluster center. Thus we can determine  $\sigma_o^2$  by looking at  $\sigma^2(r)$  at large projected radii. Figure 6 shows a plot of  $\sigma(r)^2$  in A/D units<sup>2</sup>. This data shows no evidence of the Poisson noise due to diffuse light granularity. We can set a lower limit on  $n(r)$  by noting that  $\sigma^2(r) - \sigma_o^2(r)$  is less than  $2 \times 10^{-5}$  at a radius of 16.8". We have  $n(r) = S^2(r)/(\sigma^2(r) - \sigma_o^2(r))$

$-\sigma_o^2(r))$  with  $S = 0.15$  A/D units/pixel and 1 A/D units/pixel is equivalent to 22 R magnitudes, and thus  $n(16.8'') \geq 7.5 \times 10^3$ . It follows that  $l_o$  is  $\leq 3 \times 10^3 L_\odot$ .

We stress here that we are only finding an upper limit on the fluctuations in the residual image, and therefore a lower limit on the number of objects. There is a gradient in the residual image within roughly  $12''$  of the center that artificially inflates  $\sigma$ , but beyond that the fluctuations show small variation about a constant. Any errors introduced with our shift method or PSF subtraction will only degrade this lower limit. We also note that for the unbinned data the  $\sigma^2$  increases as expected (i.e. by the number of pixels used in the binning) for the equivalent radius.

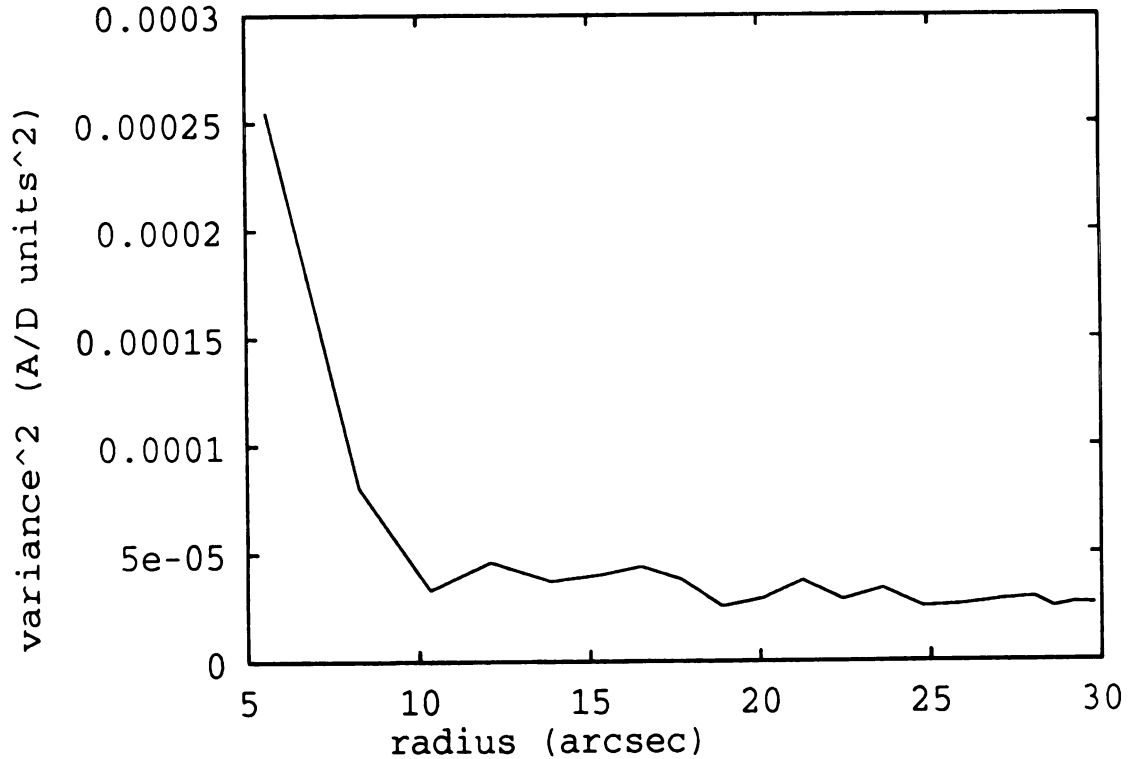


Figure 6: Square of the Variance per Radial Bin in A2670 Residual Image.

### 3.1.2 Number Density and Luminosity Function

Using the IRAF photometry data, we determined the number of objects per radial bin. Figure 7 is a plot of the object number density (points) versus radius along with a scaled version of the diffuse light profile (dashed line). There is a distinct difference in shape of the radial profiles of the diffuse light and the objects in the field for radii less than  $150''$  even after accounting for the obvious uncertainty in the number density background level. We do not confirm the similarity in number density and diffuse light profiles claimed by Oemler (1973) or Schombert (1988).

Since the integration time and S/N of our background frames differs from our data frames, we cannot remove contaminating background objects from a LF of our cluster image by using the background images. However we can use the outer part of our cluster image (i.e. outside the region we measure a significant diffuse light signal) for a background estimate. Figure 8 is just such a differential luminosity function (DLF): the LF from the outer  $150''$ - $300''$  has been subtracted from the inner  $150''$ . Also, subtracting another outer annulus  $240'' \leq r \leq 300''$  from the inner region yields a similar DLF, while subtracting two contiguous outer annuli ( $150'' \leq r \leq 240''$  and  $240'' \leq r \leq 300''$ ) yields a DLF consistent with zero. The DLF suggests that there might be some excess objects for a R magnitude/pixel brighter than 22., and a deficit for objects fainter. This deficit is based on those points between 22. and 24.5 mag/pixel, as we can not reliably measure fainter than 24.5 R mag/pixel. We make this cut-off based on a test performed to determine IRAF's false detection rate on an image of Gaussian noise having the same mean as our data. The resulting LF shows the peak of false detections to lie at 24.5 R mag/pixel, and falls off similarly to the data at fainter magnitudes.

If the LF were a separable function of radius and magnitude, then the expected

DLF should be a scaled version of, for example, the Schechter function. Clearly our DLF indicates a departure from this behavior in the innermost regions of the cluster.

### 3.1.3 Autocorrelation

Before we could perform an autocorrelation on our residual images, we had to remove all objects. We did this by blanking out (assigning a large negative number to) contiguous pixels around all objects that were 2.5 standard deviations above the image mean. Due to computing time constraints, we used  $256^2$  pixel sub-sections, one centered on the cD and four in the outermost corners of the original  $1024^2$  images. Because of the "holes" in the image, the autocorrelation had to be performed in real-space with the following equation:

$$A(\delta) = \frac{1}{N_\delta} \sum_{i,j < i} d_{ij} d_{ij+\delta}$$

where  $A$  is the autocorrelation function of the separation  $\delta$  between pixels,  $N_\delta$  is the number of measurements for each separation, and  $d_{ij}$  is the data or intensity level at each pixel with position in the image  $i,j$  that has not been blanked out. We note that typically pixels within a 20-30 pixel radius from the cluster center were removed in the blanking procedure.

Figure 9 shows the autocorrelations for the 12 frame R-band tessellation center (solid line) and 4 corners (dashed lines) for the residual image produced by subtracting the diffuse light determination. Figure 10 shows the autocorrelations for the center region in the 6 frame V-band tessellation for either residual images in which the diffuse light determination (solid line) or a fit to that determination (dashed line) were subtracted. Though not shown, the autocorrelation of the 5

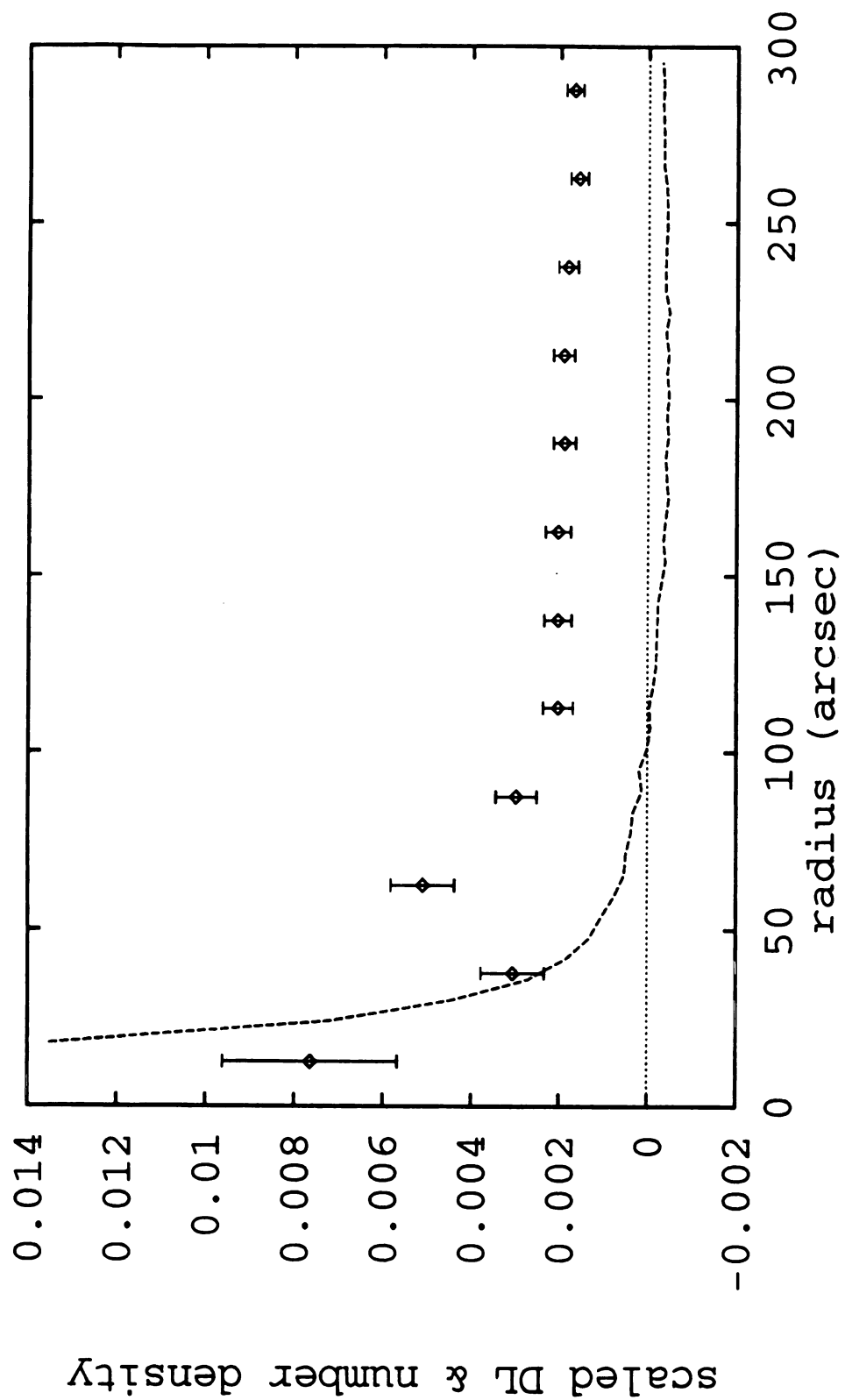


Figure 7: Object Number Density & Scaled Diffuse Light in A2670.

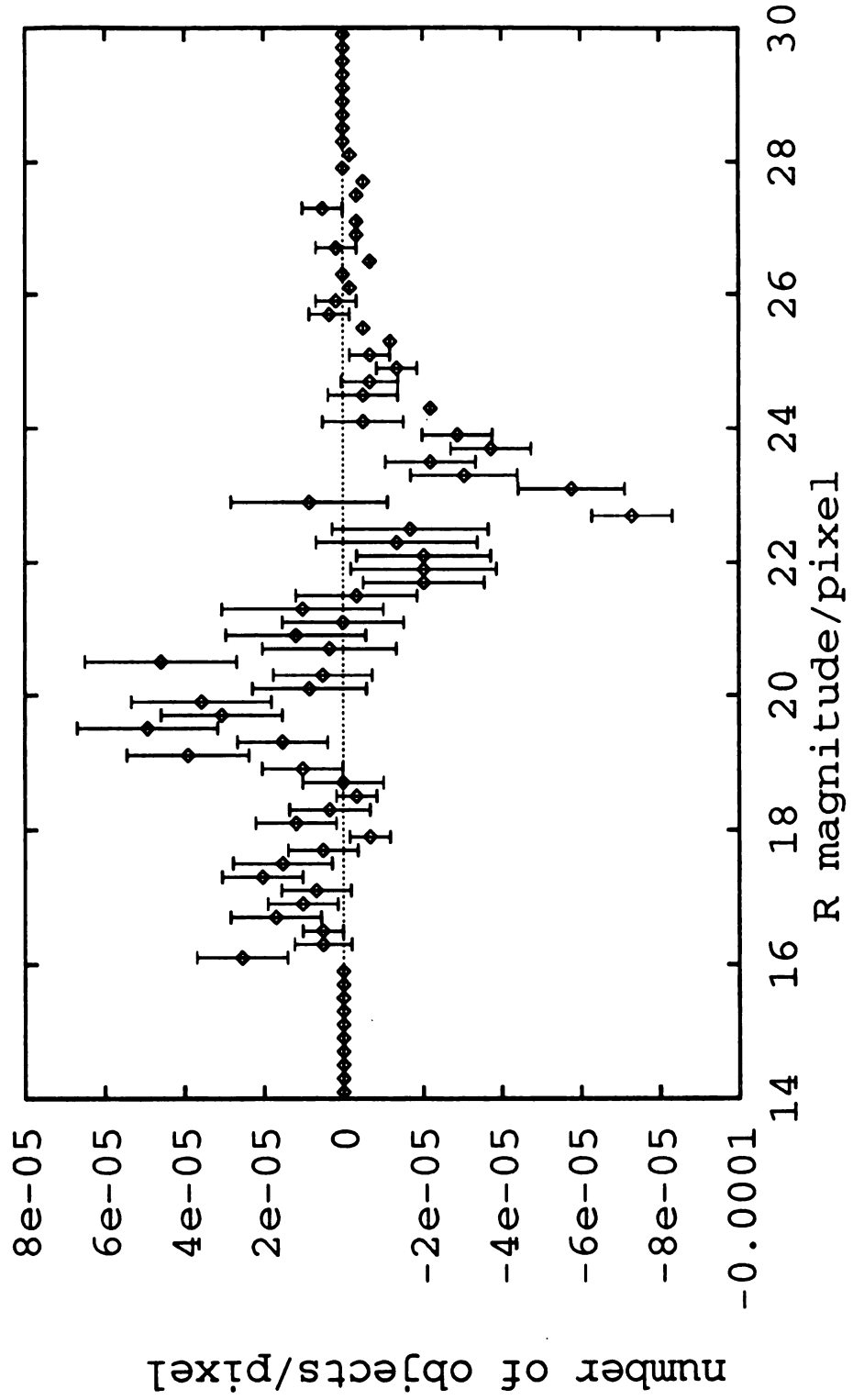


Figure 8: Differential Luminosity Function for A2670 Inner Region.

frame R-band tessellation center subsection has a similar shape and first zero crossing compared to the deeper R-band image. The autocorrelation amplitude for the center subsection is also substantially larger than that for the corner subsections of the 5 R-band frame tessellation. The diffuse light data subtracted and fit subtracted images yield autocorrelation curves that are similar in shape for any of our images. The only processing done to these curves was to subtract an offset representative of the value the autocorrelation approaches at large separations. We note here that we can never know this offset exactly because the finite size of our picture does not allow a large enough separation to be reached for the autocorrelation to truly go to a constant. We can estimate this constant to be the square of the image mean.

If the diffuse light profile were not spherically symmetric or the de Vaucouleurs' fit to profile were not representative, the effect on the autocorrelation would be seen at separations on the order of the entire frame. We tested this by subtracting the de Vaucouleurs' fit from the image offset from the true center one pixel in both perpendicular directions. The resulting autocorrelation has amplitude of roughly that of the correct autocorrelation. For lags greater than 60 pixels, there is a distinct difference in shape from the correct autocorrelation: instead of a signal oscillating about the zero-point with first crossing around lags of 60, the autocorrelation show a roughly constant value above zero until lags of 180 and then drops to a fairly large negative value at the largest lags. This test supports the significance of the results at small lags for the true autocorrelation. We do not expect any asymmetries in the profile to be as large as the one forced with this test, but, if they exist, they would not substantially effect our result for small lags.

We devised several ways to test the autocorrelation algorithm and our data reduction method. First, we autocorrelated an image of random numbers between



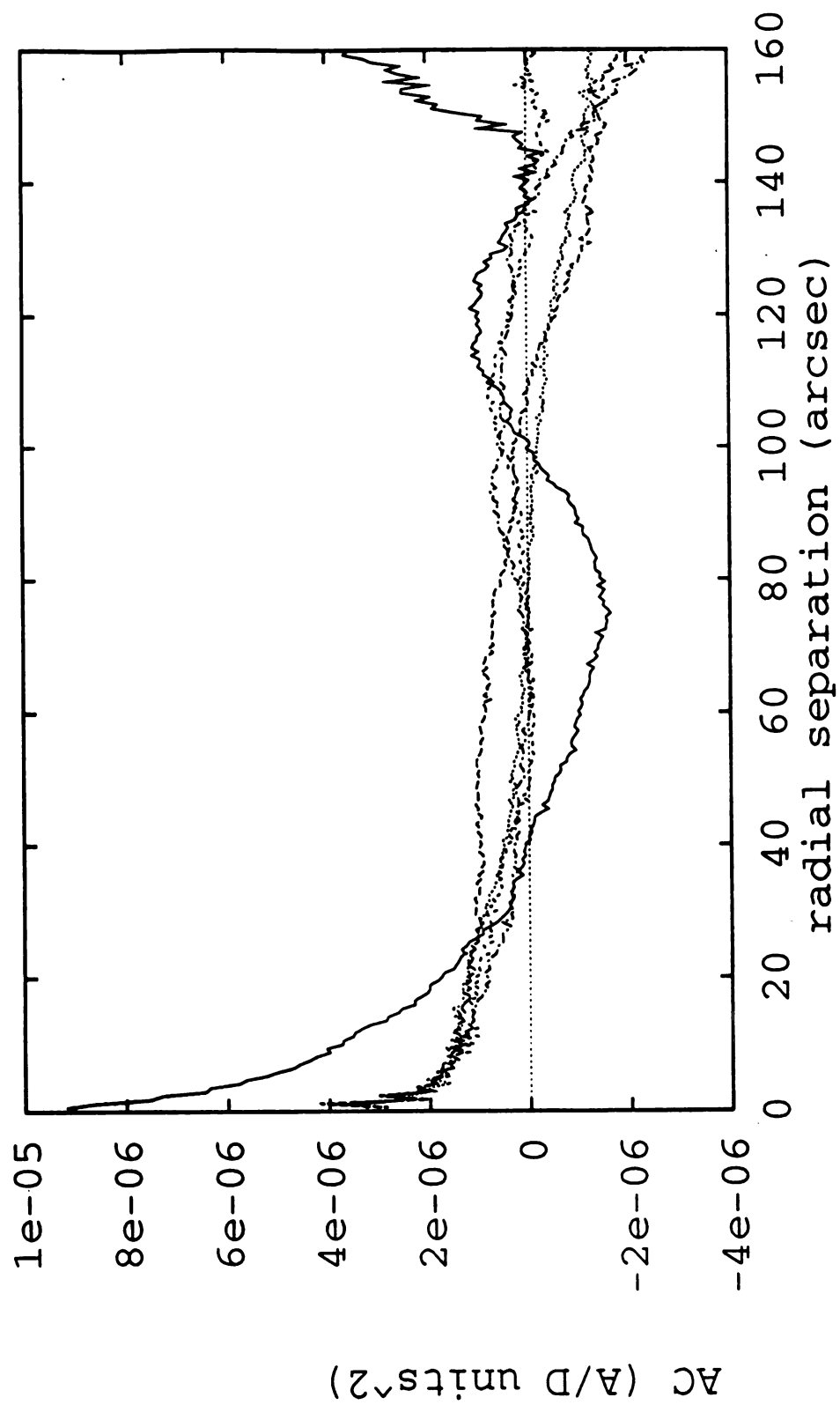


Figure 9: R-band Autocorrelations of Inner & Outer Regions of A2670.

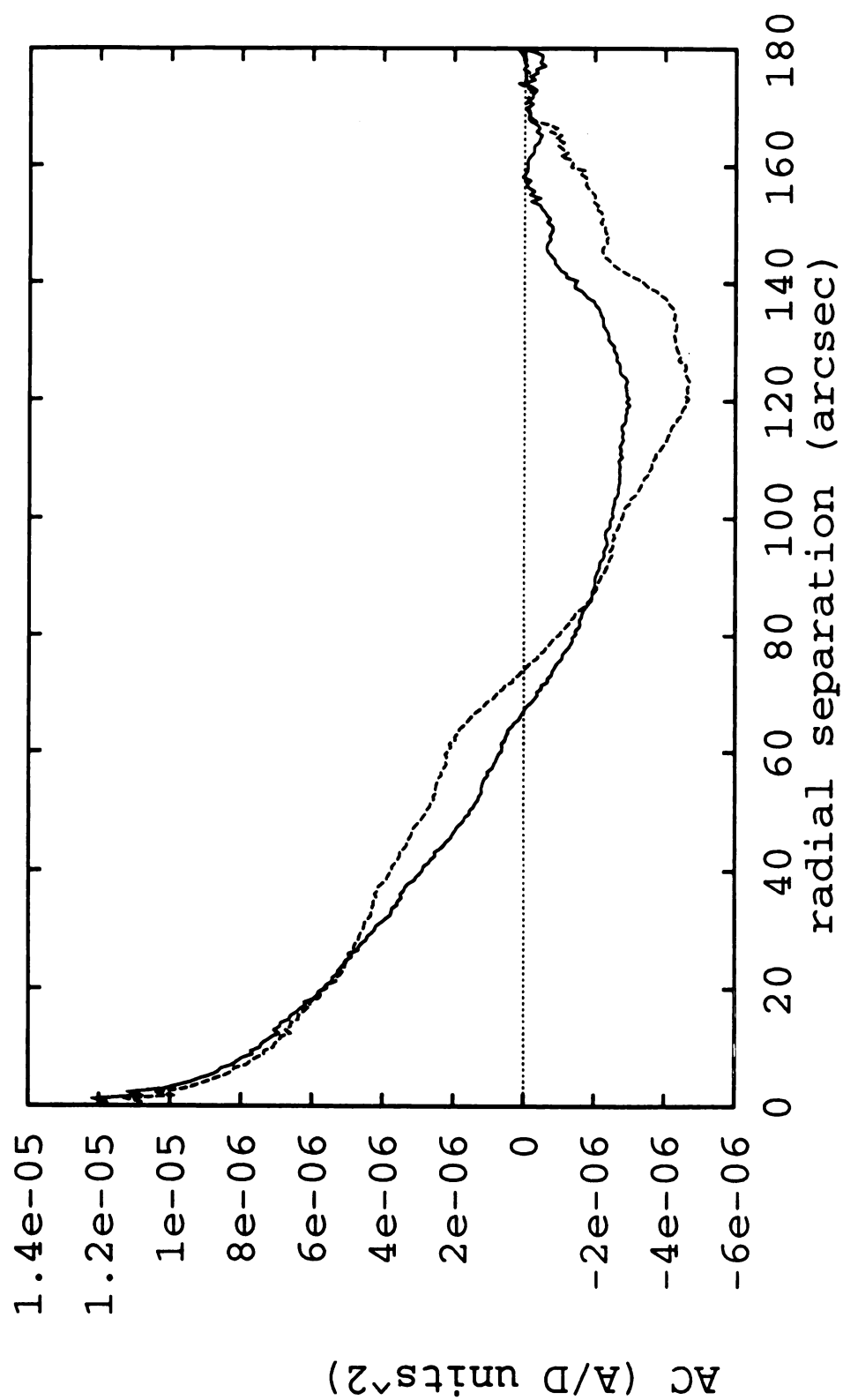


Figure 10: V-band Autocorrelations of A2670 in Data & Fit Subtracted Images.

0 and 1, which resulted in a delta function at zero-lag with the proper constant value of  $0.5^2$  for all other separations. A check on the reproducibility of our data reduction method can be seen in the fact that the two separate nights' R band observations yielded strikingly similar autocorrelation functions when either the diffuse light profile or the de Vaucouleurs' fit to the profile were subtracted. The effect of blanking out pixels was investigated in three ways. First we checked the effect of spatial "holes" over a random noise distribution. We masked an image of Gaussian noise with a pattern of holes produced for one of our cluster frames. The resulting autocorrelation was the expected delta function at zero-lag with a value equal to the mean squared for all other separations. We also changed the number and size of the "holes" by either lowering the threshold to blank pixels or by scaling the radii of blanked regions found for a particular threshold. Both have the effect of reducing the autocorrelation amplitude for small lags in the center region, but not in the outer regions. Increasing the radii of blanked regions also has the effect of reducing the amplitude at lags of roughly 30"-60", which suggests that the larger radius is required to assure our autocorrelation is not picking up scattered light from objects whose PSF's were not removed in this region.

How can we interpret this autocorrelation ? To begin to answer this question, we made images of 50 and 100 Gaussian galaxies of the form

$$G = Ae^{-\frac{(x-x_o)^2+(y-y_o)^2}{2\sigma^2}}$$

where  $x_o$  and  $y_o$  are generated randomly, the amplitude  $A$  was 2, and dispersion  $\sigma$  was 1, and the objects were superimposed on normally distributed noise with a zero mean and a RMS variation of 0.0083 (comparable to the data frames). This image was then masked with the "hole" pattern that was used for real cluster data. The

resulting autocorrelation is plotted in Figure 11. For a hundred galaxies (dashed line) the peak at a lag of 1 pixel is properly twice that for 50 galaxies (solid line). An estimate of the FWHM of the autocorrelation peak is roughly three times  $\sigma$ .

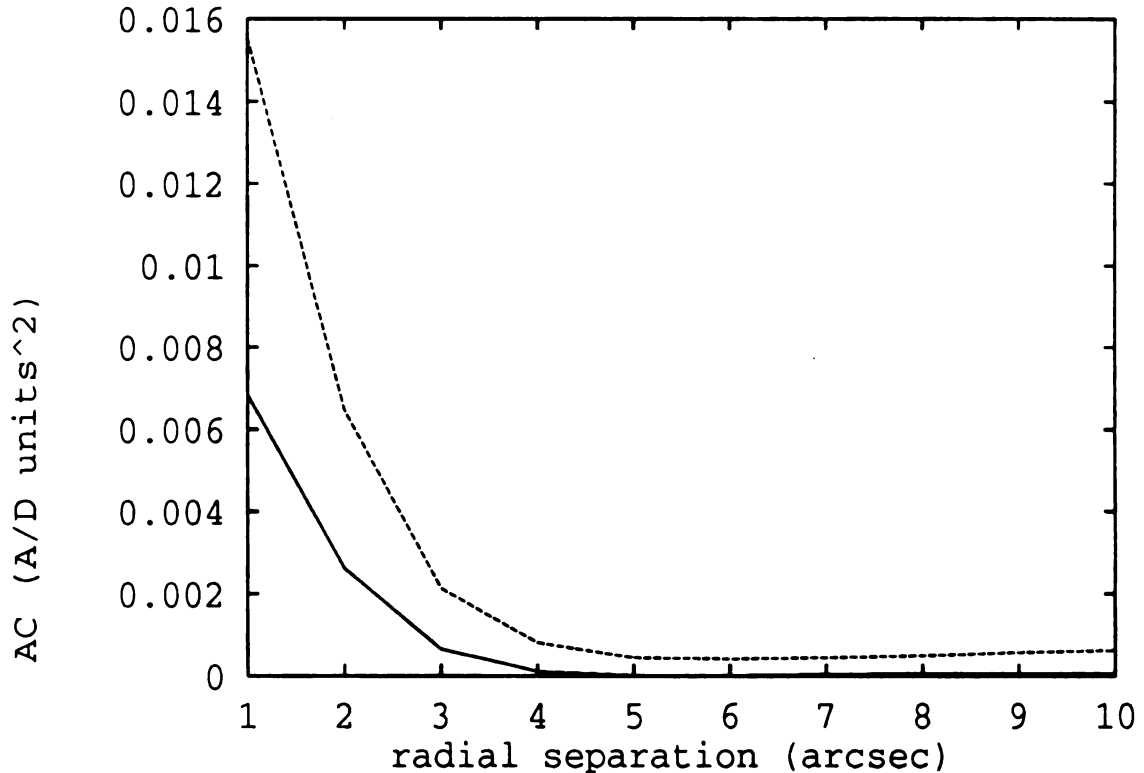


Figure 11: Autocorrelations of 50 & 100 Masked Gaussian Objects.

What does this simple model tell us about the origin of the spatial scale of the cluster autocorrelation ? First of all, if we calibrate the autocorrelation at lags of 1 pixel with the cD peak (11.07 ADU) value we find that we are measuring an effect that is less than 0.05% of the diffuse light, which is much smaller than the variance statistic per pixel we described earlier. (Though at a radius of 16.8" where

the diffuse light is 0.15 ADU, the autocorrelation amplitude is  $\sim 2\%$  of the diffuse light.) We must be careful in interpreting the amplitude at small lags because the signal we are measuring is affected by the number of pixels that are removed. The autocorrelation signal is weighted toward the center of the cluster, as is apparent from the comparison of autocorrelations of the central to the outer regions. As more pixels are de-weighted from the center of the image (where most of the "holes" lie), the autocorrelation signal weakens. However, we may be able to compare the amplitude of the autocorrelation to what is expected if the objects represent the faint end of the LF. This calculation is done for both A2670 and A2029 in section 4.2.2.

At this low level, large scale (of order the CCD frame size) errors in our photometry (e.g. zodiacal light and extinction coefficients) could exist. Thus the mean pixel value in a  $256^2$  subarray may be biased, so that the large scale information in the autocorrelation function is probably not reliable. Such errors appear as a zero-point offset and spurious correlation amplitudes at large lags where there are also significantly fewer pixels at these separations. We are encouraged by the agreement in the form of the V and R autocorrelation data at lags less than about  $1'$  (allowing for a small offset error between the two colors).

While the autocorrelation function is noisy we can extract at least one piece of information from these curves: a spatial scale. Our technique for removing objects affects the amplitude of the autocorrelation at small lags. Scattered light from these objects for which no PSF subtraction was performed affects the autocorrelation amplitude at lags of  $30''$ - $60''$ . Hence, an estimate of the FWHM of the autocorrelation will be biased. Instead, we can safely characterize the "clumpiness" of the material causing the diffuse light fluctuations with an exponential scale length of about 20-30

pixels (for lags less than 30"). This scale is independent of all the tests we have performed with the data and corresponds to a clump size of 13-20/h kpc. We emphasize this length must be interpreted as a size not a separation between objects. The latter scale would be measurable as the distance between the zero-lag and a secondary peak in the AC. Our half-length would describe a separation only if the widths of the objects were larger than their separations, which does not seem likely.

### 3.1.4 Color

Next we investigated the color of the objects in our images, including the cD. By matching photometry list coordinates of objects in the 5 frame tessellation in R and the 6 frame tessellation in V, we generated a list of approximately 320 objects for which we could produce a color (V-R) histogram (Figure 12a). We also produced a similar histogram for single background frames located 30' north of the cluster (Figure 12b) for comparison. The color of sky is roughly 0.35 magnitudes. K corrections at this color were approximated with the relation  $\delta(V-R) \sim -z$  (Sandage 1972), where  $z$  is the redshift. We estimated a zero interstellar reddening from the HI maps of Burnstein & Heiles (1982); A2670's galactic latitude is approximately  $68^\circ$ . We measured the color of the cD to be 0.72 using the flux within a radius of 18" about the cD in both R and V frames. As is apparent from Figure 12a, the cD color lies near the peak of the histogram for the cluster.

We also measured the color gradient in the halo. We can compute the halo color with the diffuse light measurements (Figure 13). There is roughly a drop of 0.6 magnitude over radius of 1.5'. When the error in the zero levels of the two frames is included, the gradient ranges from 0.4 to 0.8 mag. We take the 0.6 ( $\pm 0.2$ ) mag decrease in V-R over 1.5' to be the gradient in the halo.

### 3.1.5 Wakes

By observing the wake of a massive galaxy, we could calibrate the gravitational diffuse light response to learn about the transverse velocity and mass of the moving galaxy. Calculations of the shape and density enhancements of such wakes are promising (Weinberg 1989, Mulder 1983). If the diffuse light has a velocity dispersion comparable to or less than the galactic dispersion, then local diffuse light surface brightness enhancements of a few percent are expected. More specifically overdensities of 3-5% in the diffuse light should be measurable and distributed approximately in a dipole pattern about the impinging galaxy. We attempted to identify candidate galaxies by looking for a dipole-like distribution in their surface brightness. Lauer (1988) reports possible wake detection around galaxies in A2199, A1185, A779, and A1126. The appearance of his candidates is very similar to theoretical predictions of Weinberg (1989). Using contour plots, we looked in the residual image for any galaxies whose center was offset from the contour center or had plume-like features associated with them. The 12 frame tessellation showed that the outermost contour (indicative of the frame noise level) of the candidate galaxies was just above the 5% level of the diffuse light at that radius. In an effort to increase the S/N, we added the 12 and 5 tessellation frames, measured and subtracted the diffuse light profile, and again looked for wakes. The S/N level in this super-tesselated frame was at best 3%, which is barely sufficient for a wake detection. Out of the 4 candidates within 20", we found none with a significant difference in central galaxy position with respect to the center of the surrounding contours.

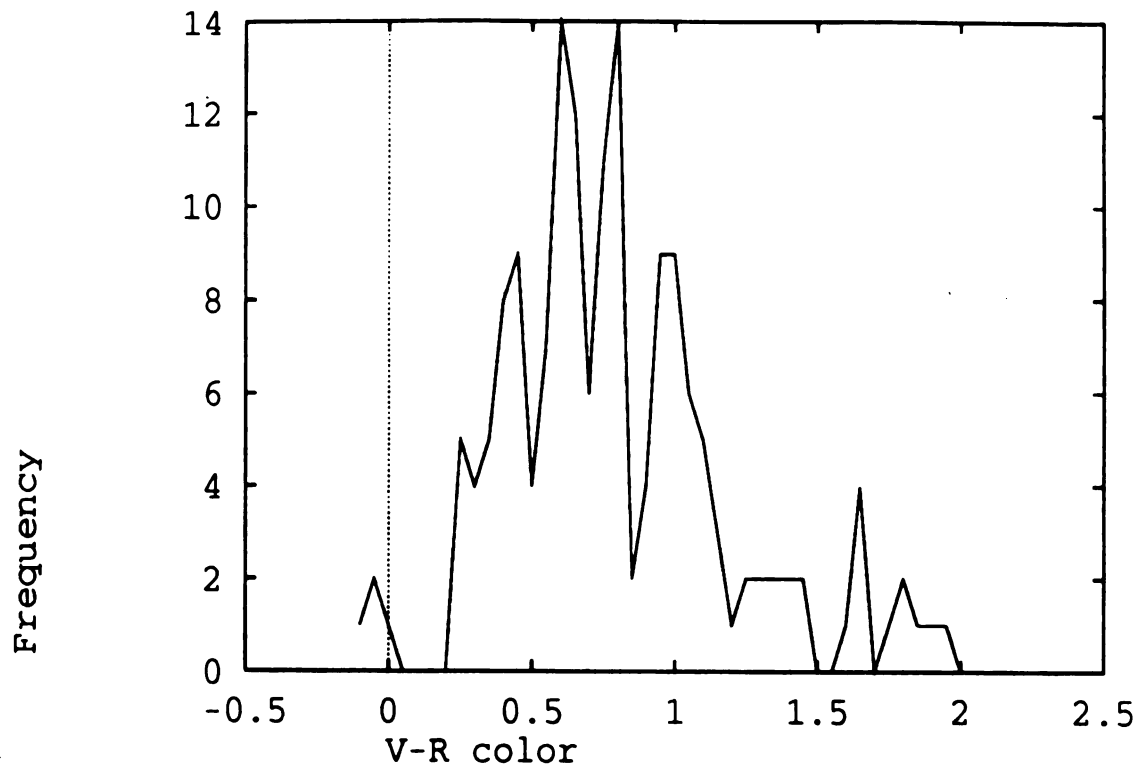


Figure 12a: Histogram of V-R Color of Objects in A2670.

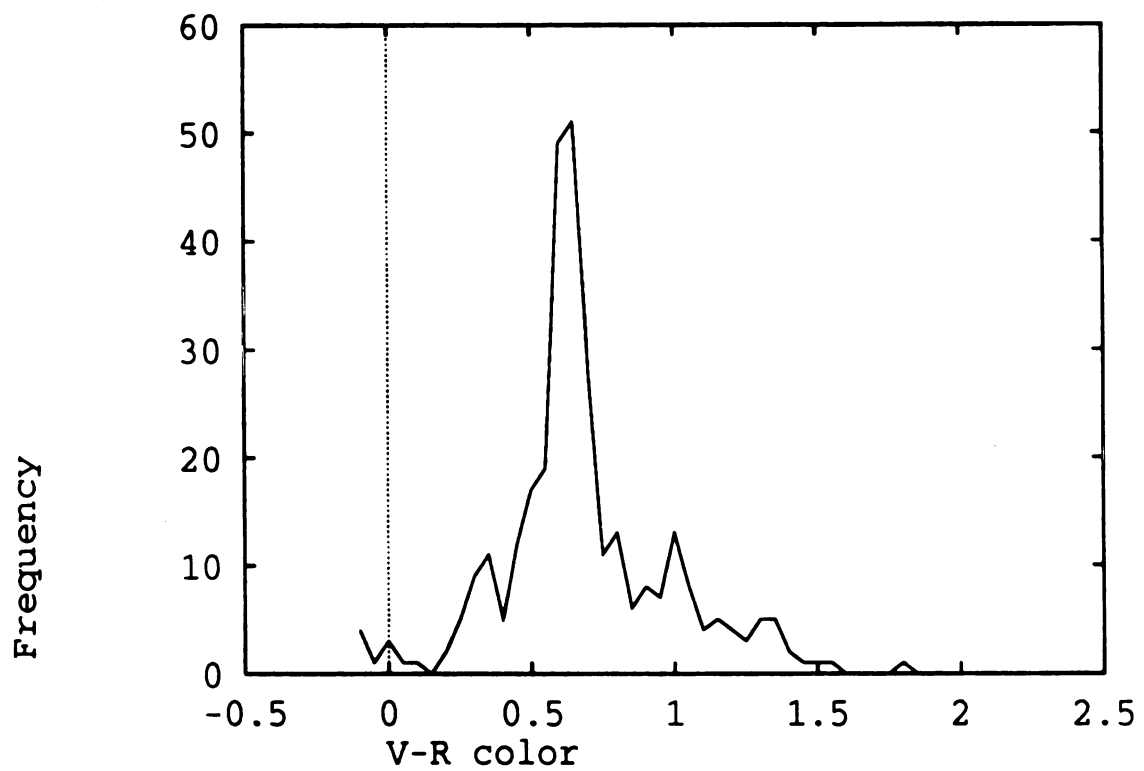
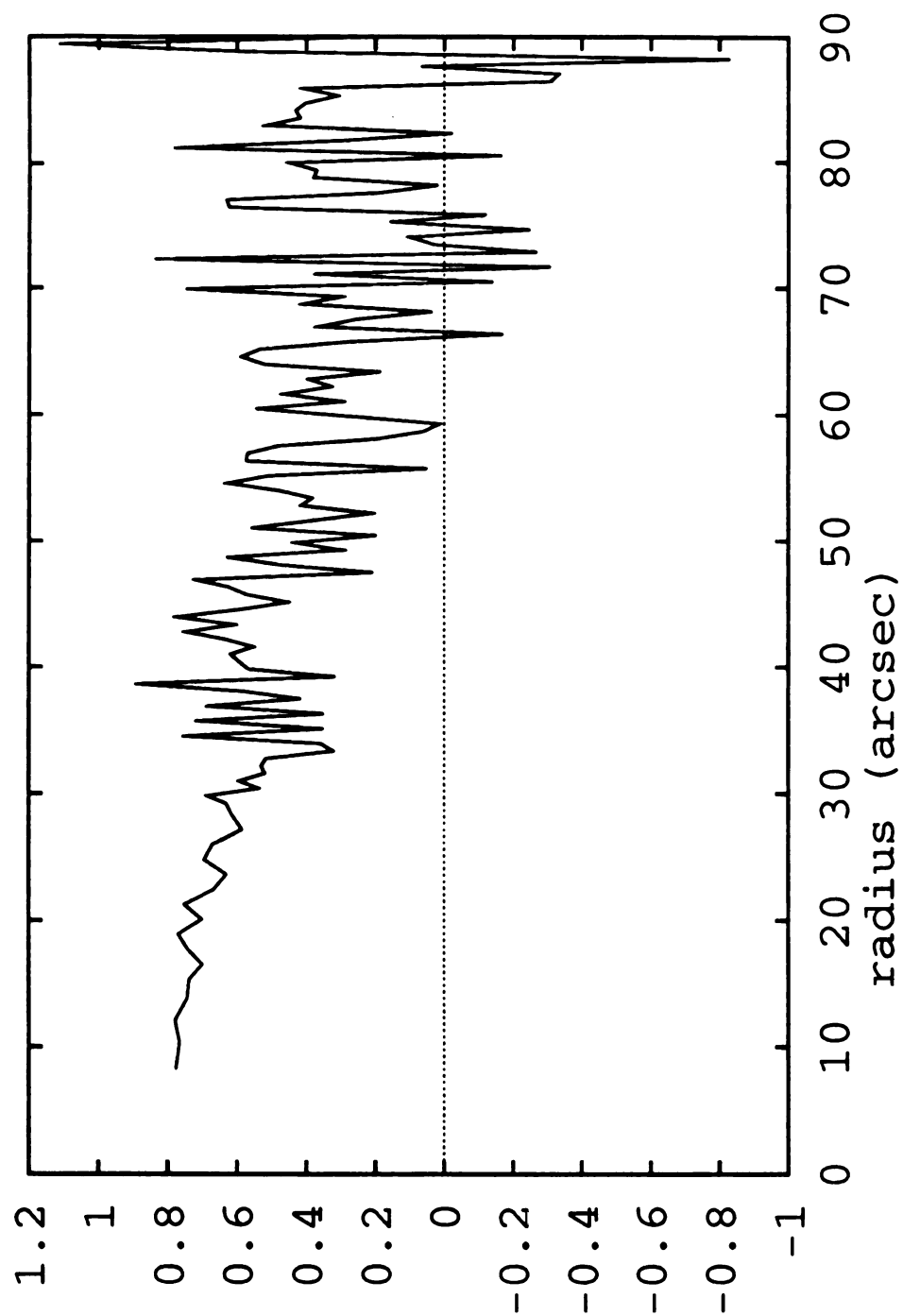


Figure 12b: Histogram of V-R Color of Objects in Background Frame.





V-R magnitudes

Figure 13: V-R Color of the A2670 Diffuse Light.

## 3.2 A2029

### 3.2.1 Diffuse Light Profile

Figure 14 shows our deepest ( $\sim 2$  hr) R-band tessellated image of the central  $4.55' \times 4.50'$  of A2029. The faintest objects visible in this figure are roughly 20.6 R mag/arcsec<sup>2</sup>. Figure 15 is a contour map of roughly the inner 1 arcmin<sup>2</sup>. The lowest contour is about 0 A/D units, and the contour interval is 400 A/D units. The tick marks in this figure denote pixels. We note that the isophotes have ellipticity which varies from 0.85 for a long axis greater than  $20''$  to roughly 1 (or circular) in the center. UBK report a constant ellipticity of 0.90 at all radii.

The purpose of taking yet another data set on such a well studied cluster was to search for and measure any anisotropy in the diffuse light profile found by UBK to be very smooth. We observed only the center of the cluster in order to maximize the S/N; hence our frame covers only roughly the inner 4.5 arcmin<sup>2</sup> or only 1/3 the extent of the diffuse light profile. We measured the diffuse light in two ways. First we used UBK's statistical method, described previously as applied to A2670, with bins of a constant ellipticity 0.85 for long axes greater than  $20''$ . We are able to measure out to a long axis of about  $150''$  before the number of pixels is insufficient. As shown in Figure 16, the resulting profile (solid line) could be used to calibrate our image against the UBK measurement (dashed line) for the range 20-100'', the upper limit being the point at which scattered light contaminates the profile. We note that the lack of an estimate of background does not effect the calibration. The residual image formed from the subtraction of this profile was used to perform the surface brightness fluctuation analysis and to look for wakes.

Surface brightness fluctuations were computed in the same manner as described for A2670. The image was binned 4x4 in order to again consider a roughly 1 kpc<sup>2</sup>

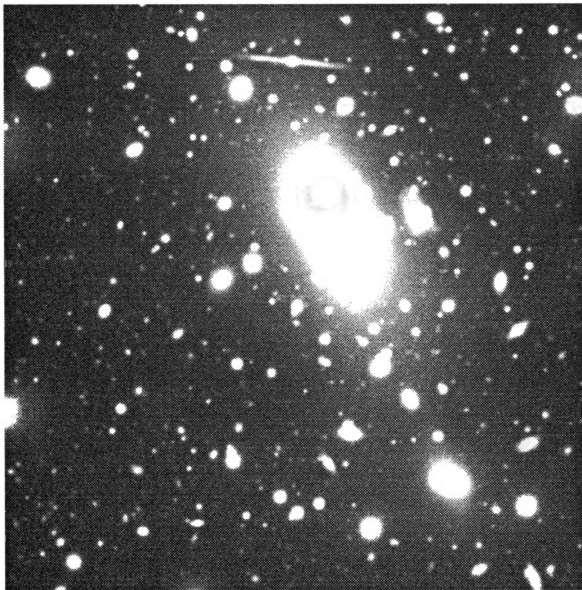


Figure 14: Gray-Scale Image of the Central  $4.5 \text{ arcmin}^2$  of A2029.

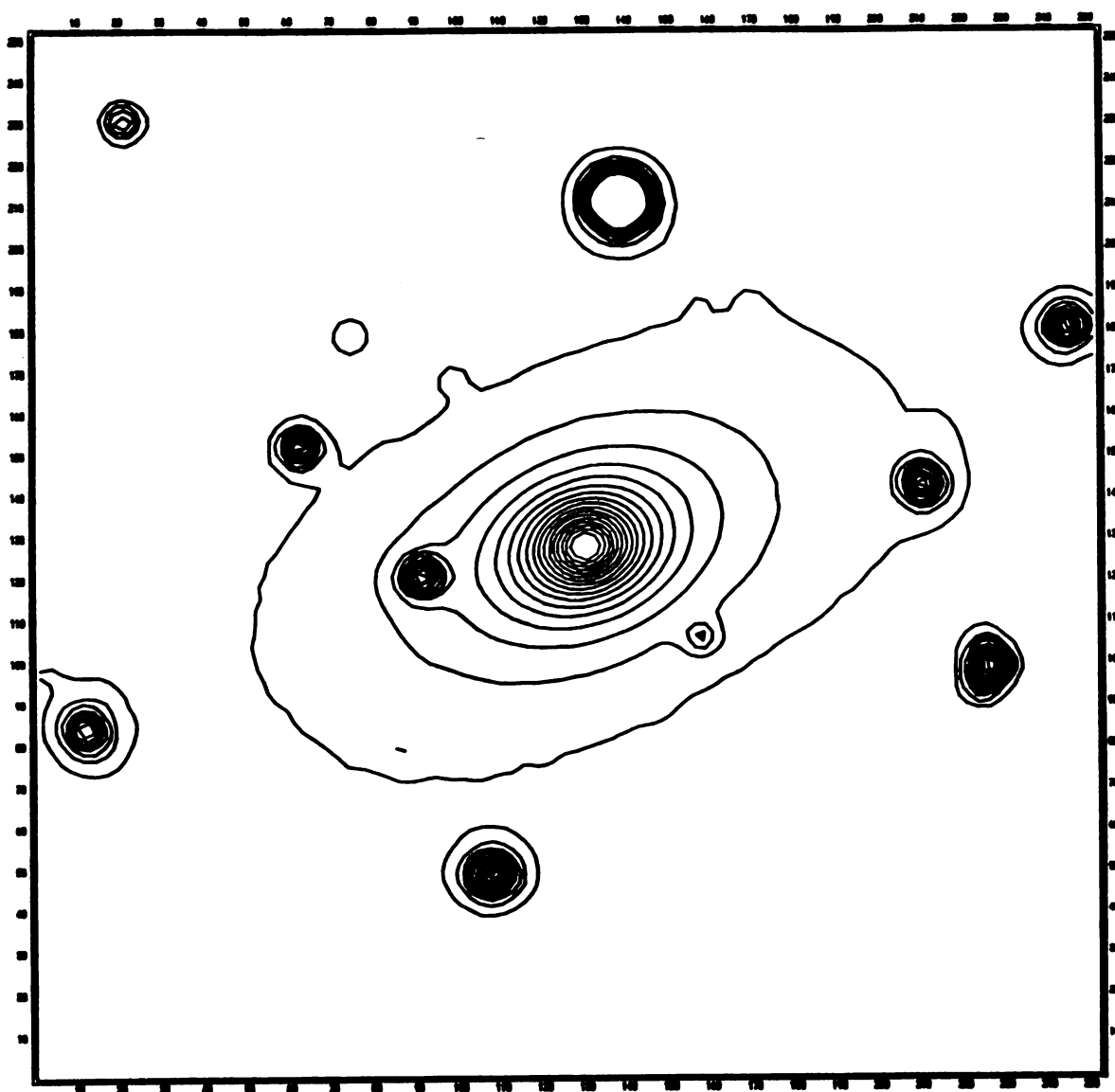


Figure 15: Contour Map of the Inner 1 arcmin<sup>2</sup> of A2029.

super pixel. In this binned image, we are only able to measure fluctuations for a long axis greater than 90 pixels. The diffuse light signal is roughly 45 A/D units, and the magnitude of the fluctuations is less than 7; thus the number of objects must be greater than 290. With our calibration per pixel ( $26.68 - 2.5\log(\text{A/D units})$ ), the luminosity per pixel is roughly  $7.6 \times 10^7 L_{\odot}$ . Hence the luminosity per object must be less than  $3.2 \times 10^5 L_{\odot}$ .

The second method of determining the diffuse light was necessary for the autocorrelation analysis. As the ellipticity is a function of radius and a PSF is not available, we needed a way to remove the diffuse light and scattered light from bright objects. The technique is simply to perform a variable radius aperture smoothing on an image in which the seeing disk of objects excluding the cD itself are masked (i.e. not included in the calculation). At each pixel, a robust average of pixels was computed in a circle of the chosen radius. The aperture radii used were 3, 6, 9, 12, 15, 21, 27, 33, 39, and 45 pixels (the last of which is roughly  $1/25$  of the  $256^2$  frame used in the autocorrelation). The resulting smoothed images were subtracted from the original image, and the remaining "seeing disks" were masked before the autocorrelation was performed. The innermost regions of the resulting images were less well represented by the larger aperture radii, but no large scale gradients were apparent, and the regions for which this method had trouble were also masked.

### 3.2.2 Autocorrelation

Figure 17 shows autocorrelations when using the smoothing technique with variable aperture radius for a  $256^2$  pixels region about the center of the cD in A2029. Figure 18 shows autocorrelations for a region furthest from the cD on the same frame (the cD and center of this subsection are separated by 610 pixels). The ten lines shown each figure correspond to the ten different radius apertures

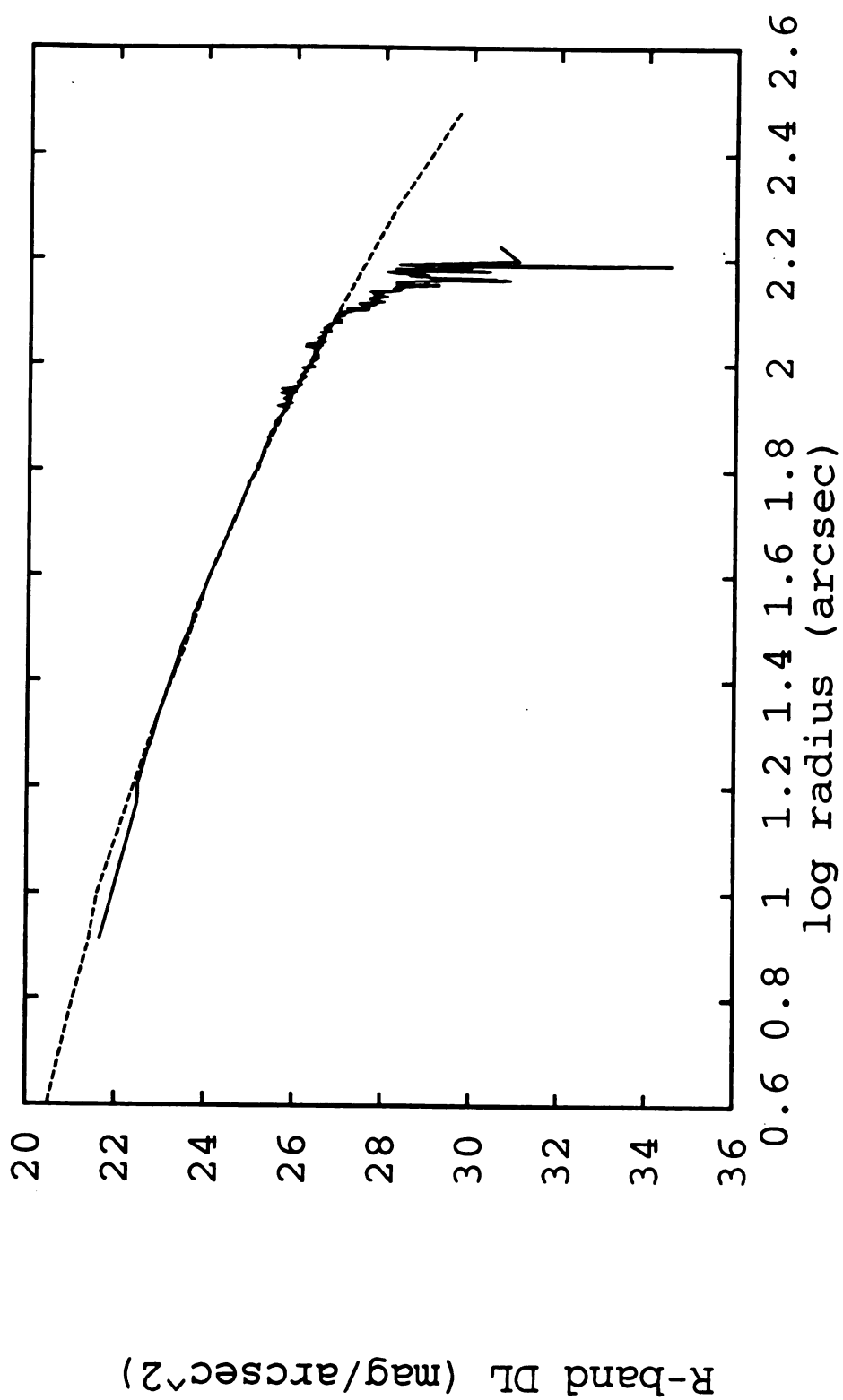


Figure 16: Our and UBK's R-band Diffuse Light Profile of A2029.

used in the smoothing procedure. We note that the autocorrelation of the center region maintains the same shape but increases amplitude with increasing aperture radius until a radius of 45 pixels. For the outer regions, the amplitude and shape remain roughly the same for all aperture radii. The autocorrelations for the inner regions are somewhat dependent on the aperture radius, but they are not likely to do be due to large scale gradients in the image because their overall shape does not change. The effects of gradients may be becoming apparent at lags of 8-16" for larger aperture radii. We can determine another exponential scale length: 17 pixels or 4.5" which is roughly the same for all aperture radii choices less than 45 pixels.

For the sake of comparison, we performed this technique on our deepest A2670 tessellation. We again find a distinct difference in the amplitude and shape of the autocorrelation for inner and outer subsections (Figures 19 and 20, respectively). Again there is an increase in amplitude with increasing aperture radius, but not as pronounced as that for A2029. The amplitudes of the autocorrelation are not easily comparable because of the difference in number of pixels that were removed in the masking procedure. We can get a rough estimate for lags of 1 pixels by "un-normalizing" or multiplying the available number of pixels separated by 1. The resulting numbers are the same order of magnitude. The exponential scale factor determined from this method is only roughly 5.4 pixels or 3.2", which is substantially less than the 24 pixels or 14" obtained from the previous method.

We would like to compare the amplitude of the autocorrelation at small lags to what we might expect from contributors representative of the faint end of the LF. Assuming a single galaxy with constant surface brightness  $s$  and  $n_{r_o}$  pixels within that galaxy separated by  $r_o$ , then the autocorrelation at  $r_o$  should be  $\sim n_{r_o}s^2/N_{r_o}$ , where  $N_{r_o}$  is the total number of pixels separated by  $r_o$ . For small objects  $n_{r_o}$

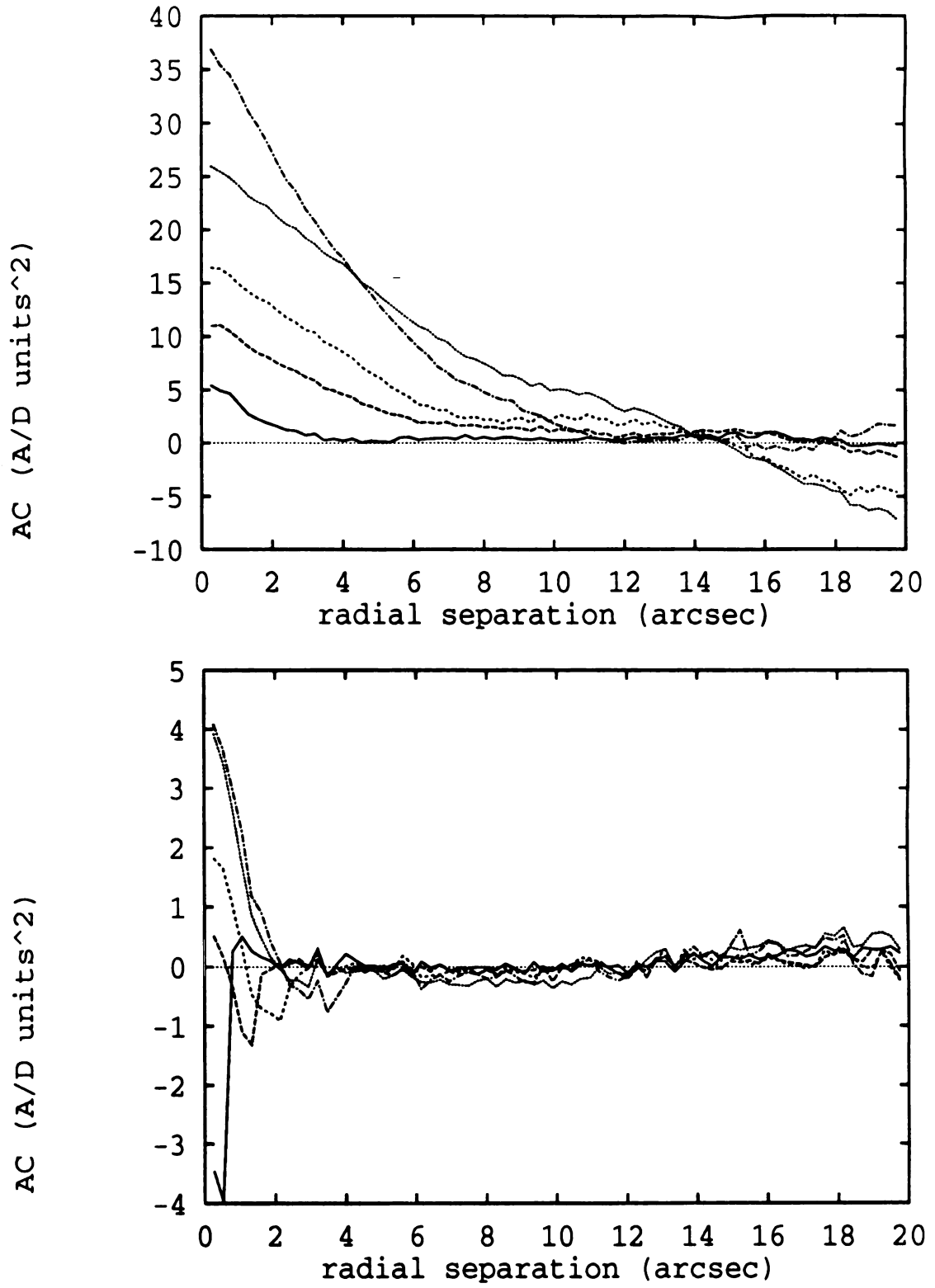


Figure 17: Autocorrelations of the Inner Region of A2029.



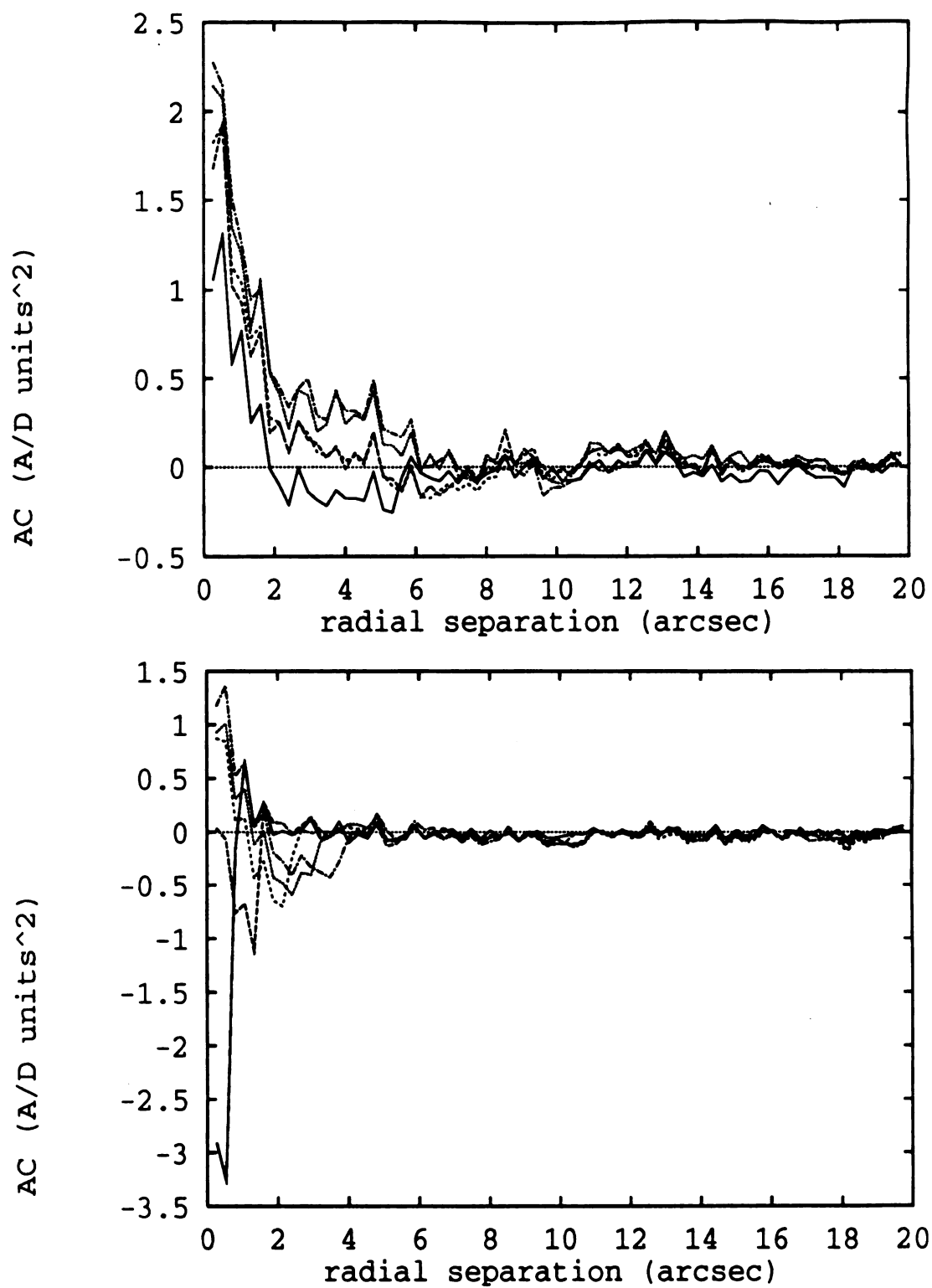


Figure 18: Autocorrelations of the Outer Region of A2029.

should go roughly as the area of the object. For  $N$  galaxies (separated by much more than  $r_o$ ) of varying surface brightness and area, we have to integrate from the detection limit of our frame to zero brightness. Expressing the surface brightness as the luminosity per area ( $L/A$ ), we need to calculate the following integral:

$$\int_0^{L_{lim}} \frac{L^2}{A} \phi(L) dL$$

where  $\phi(L)$  is the number of objects at a given luminosity, i.e. the LF. We will ignore for now the fact that our DLF for A2670 suggests a lack of faint objects, and use a Schechter LF which has the following form:

$$\phi(L) = \frac{N_o}{L_*} \left( \frac{L}{L_*} \right)^\alpha e^{-L/L_*}.$$

where  $N_o$  is normalization factor,  $L_*$  is a characteristic luminosity of the cluster and  $\alpha$  has been determined empirically to be roughly -1.25 (although some studies support -1.50) for almost all clusters. Dressler (1978a) has determined LF for both A2670 and A2029 in the F band for  $\alpha = -1.25$ . In order to convert from F to R bands, we need a B-V color for our cDs. The V-R color for A2670 is 0.72, and from Mackie (1992), V-R for A496 is 0.70, and B-V is 1.15. Also Oemler (1974) finds that galaxies with late-type spectra have a  $J-F = 1.1 \pm 0.10$ , which supports our assumed B-V color of 1.15. We can convert Dressler's characteristic F-band absolute magnitude into a R-band  $L_*$ : for A2670 it is  $6.9 \times 10^{10} L_\odot$ , and A2029,  $2.7 \times 10^{10}$ . We also need values for  $N_o$ . Dressler chooses them such that the observed total number of galaxies in his sample is returned when he integrates his LF. Doing this integration, we find  $N_o$  for A2670 is 51, and for A2029, 142. For  $L_{lim}$ , we use the brightness of the faintest detected object as found by IRAF: 29.2 R mag/arcsec<sup>2</sup>

for A2670 and 25.8 for A2029. Now we can compute the following integral with the simplifying assumption that the area of the contributing galaxy is not function of luminosity:

$$\frac{N_o L_★}{A} \int_0^{L_{lim}/L_★} x^{\alpha+2} e^{-x} dx.$$

The integral can be done numerically with a Romberg integrator (Press et al. 1992). Combining all these quantities, the expected autocorrelation at small lags should be  $0.011/A$  for A2670 and  $7.8 \times 10^5/A$  for A2029 if that signal is due to the faint end of the Schechter LF. The autocorrelations shown in the figures all have been normalized by the number of pixels at each separation. For A2670, there are roughly 82,000 pixels separated by 1 pixel used in the autocorrelation with smoothing aperture radius of 33. For A2029, there are roughly 72,000 for an aperture radius of 39. Multiplying these normalization factors by the average amplitude, we have 0.276 for A2670 and  $1.87 \times 10^6$  for A2029.

We have yet to deal with the area of the contributing faint objects. The exponential scale factor is obviously too large; the faintest object IRAF detects has a radius of roughly a few pixels. The important question is whether or not we can estimate the number of pixels separated by lags of 1 as the area and then treat the area as independent of luminosity. As the luminosity get smaller, the area gets smaller, and the integral goes to zero, suggesting that the largest objects contribute most to the integral. We can not have an area less than one as these calculations might imply when compared to what is observed. Unfortunately, the integral is somewhat sensitive to detection limit: a change in the magnitude to 28. (from 29.2) increases the result to  $0.077/A$  for A2670. We may have to be satisfied that this simple calculation yields a ballpark figure comparable to the measured amplitude

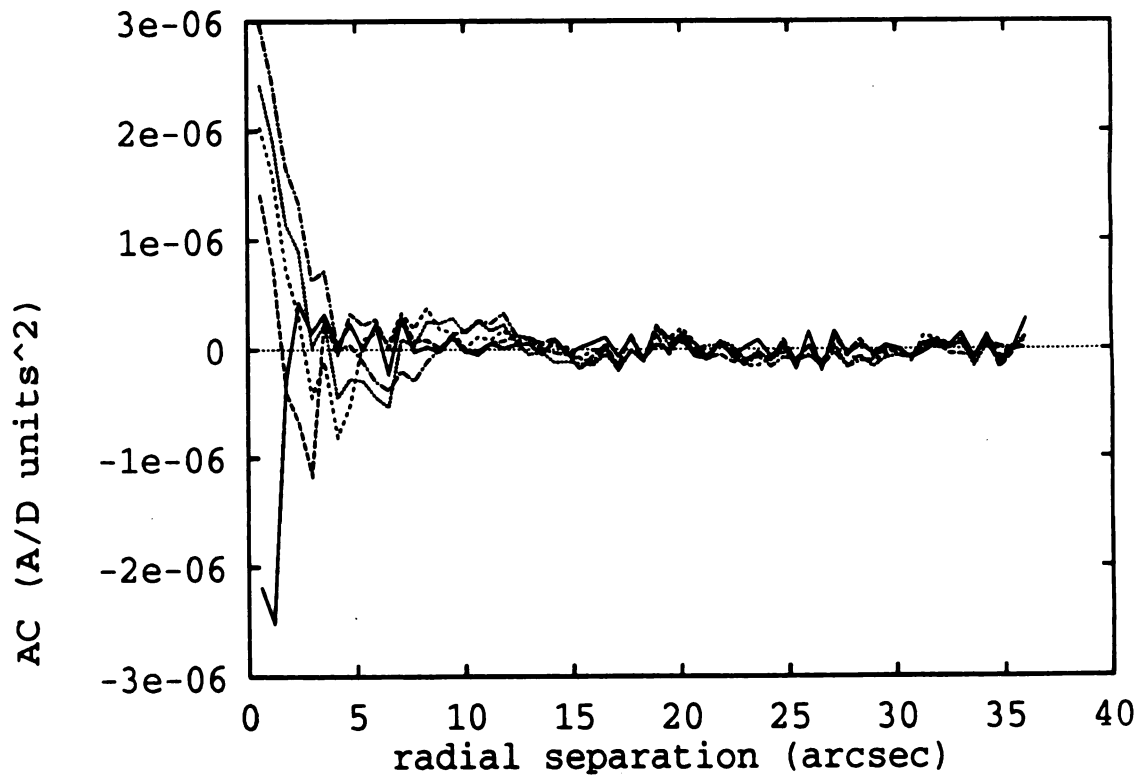
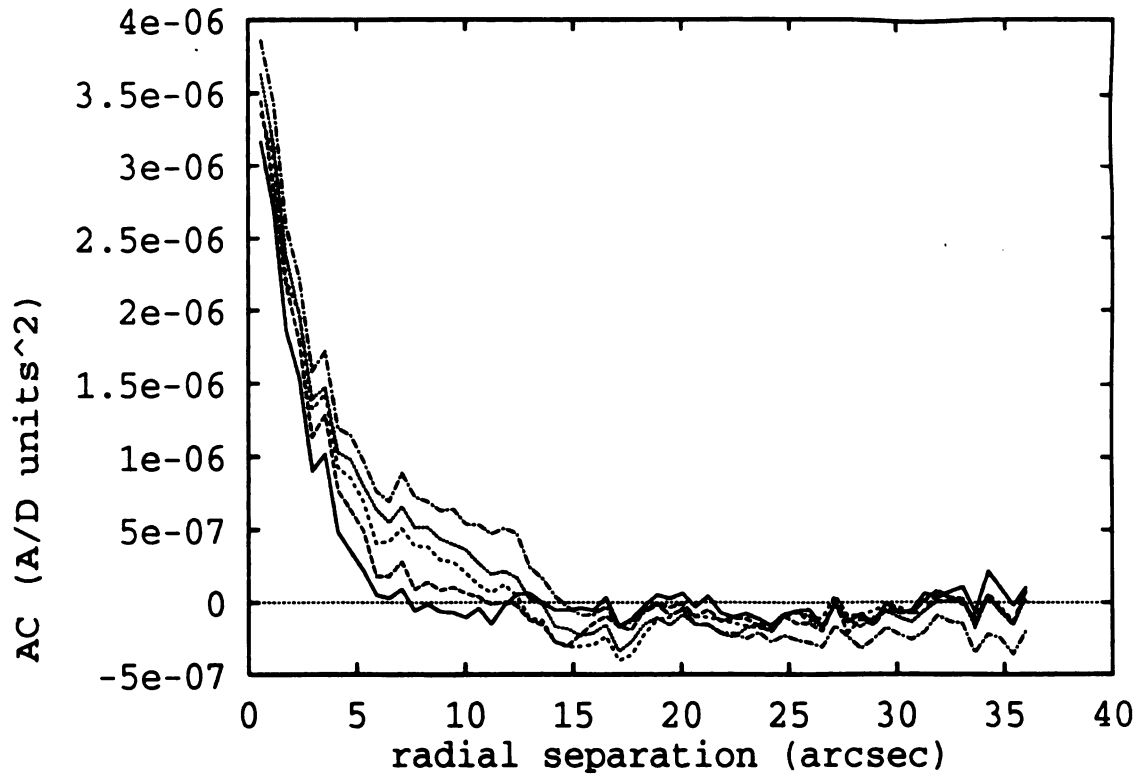


Figure 19: Autocorrelations of the Inner Region of A2670.

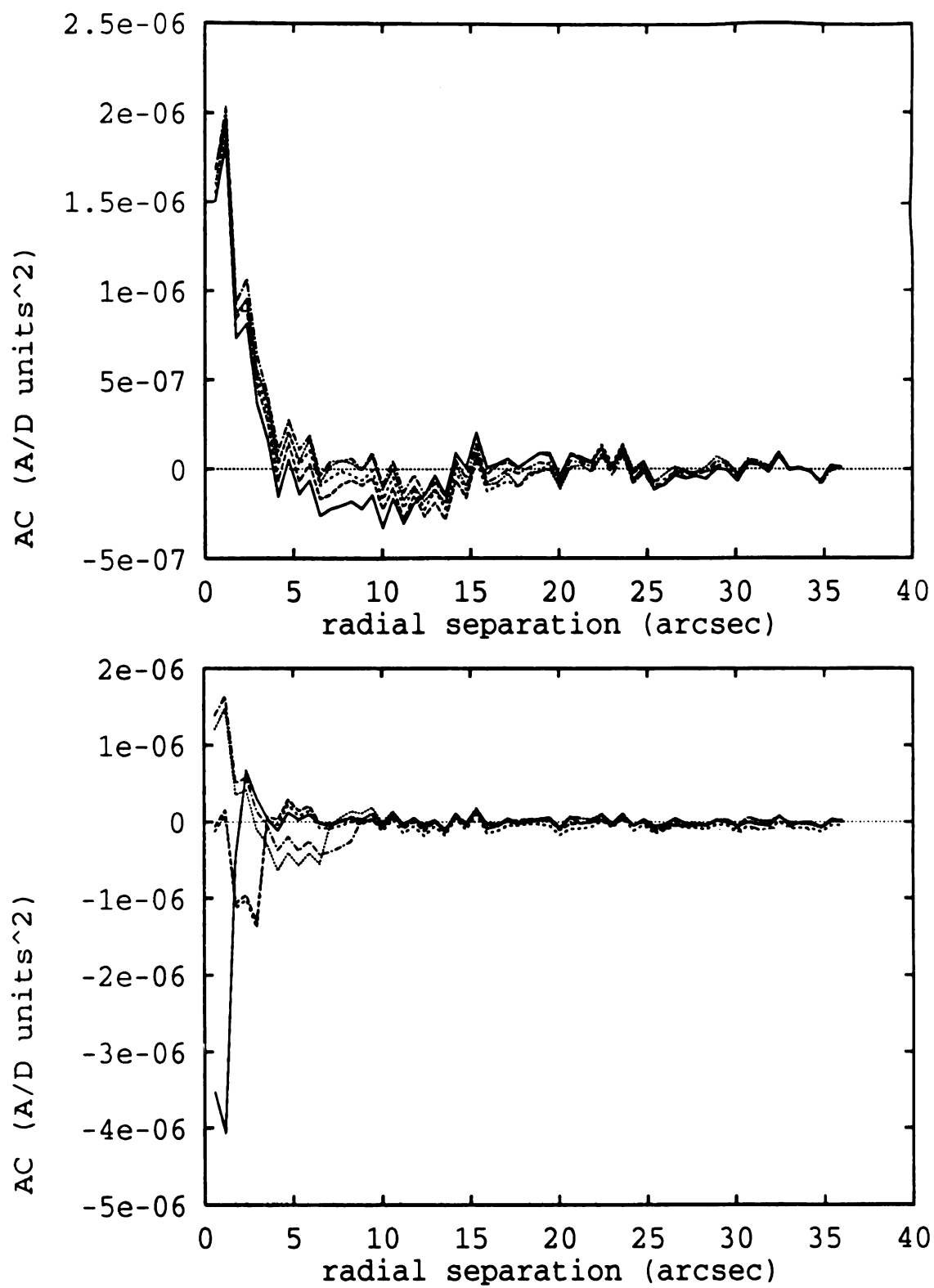


Figure 20: Auto-correlations for the Outer Region of A2670.

(especially considering the guestimates involved) until more sophisticated methods can be performed (e.g. a Monte Carlo calculation).

### 3.2.3 Wakes

We report the possible detection of wakes in deepest image of A2029. Five galaxies have plume-like features associated with them, similar to those reported by Lauer (1988). These features are just visible in our second image of A2029 with its poorer S/N. Figure 21 shows the outermost contours of the candidate galaxies with the direction to the cD indicated with an arrow. We note the distinct curvature of isophotes which is very similar to the simulations of Weinberg (1989). With the exception of the third and fifth candidates, the wakes are oriented with a larger radial component than tangential with respect to the cluster center. The lowest isophote in each of these contour plots is roughly 0, and the interval is 25 A/D units. These features range from 5 to 150% of the diffuse light level in their vicinity. Table 1 lists the following simple wake characteristics for candidates 1 through 5: the distance from the cD ( $R$ ), diffuse light value at the galaxy position ( $DL$ ), an estimate on the projected radius of the galaxy ( $r_g$ ), the length of the wake ( $l_w$ ), the magnitude of the galaxy ( $m_g$ ), and that of the wake ( $m_w$ ). The wake luminosity was computed by averaging those points above the mean galaxy profile. The brightest wake is only  $\sim 10^{-2.5}$  its parent galaxy. The galaxy profiles do not show any evidence of being abnormal in any other way: for instance, less peaked, as might be expected if significant material were stripped away from the center.

There are velocity measurements for two of the candidates (Bower et al. 1988). Candidate 3 has a small radial velocity above the cDs (390 km/s) as compared to the cluster dispersion of  $\sim 1430$  km/s, which could suggest that much of the motion is tangential, and if the direction of the plume is any indication, then the motion is

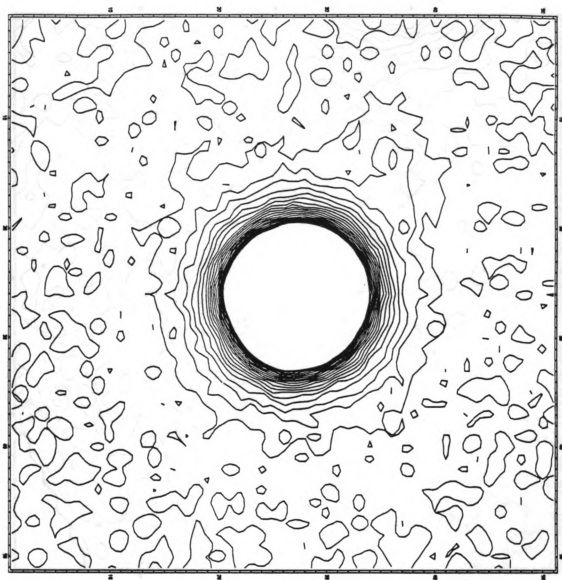


Figure 21: Contour Maps of Candidate Wakes, Candidate 1.

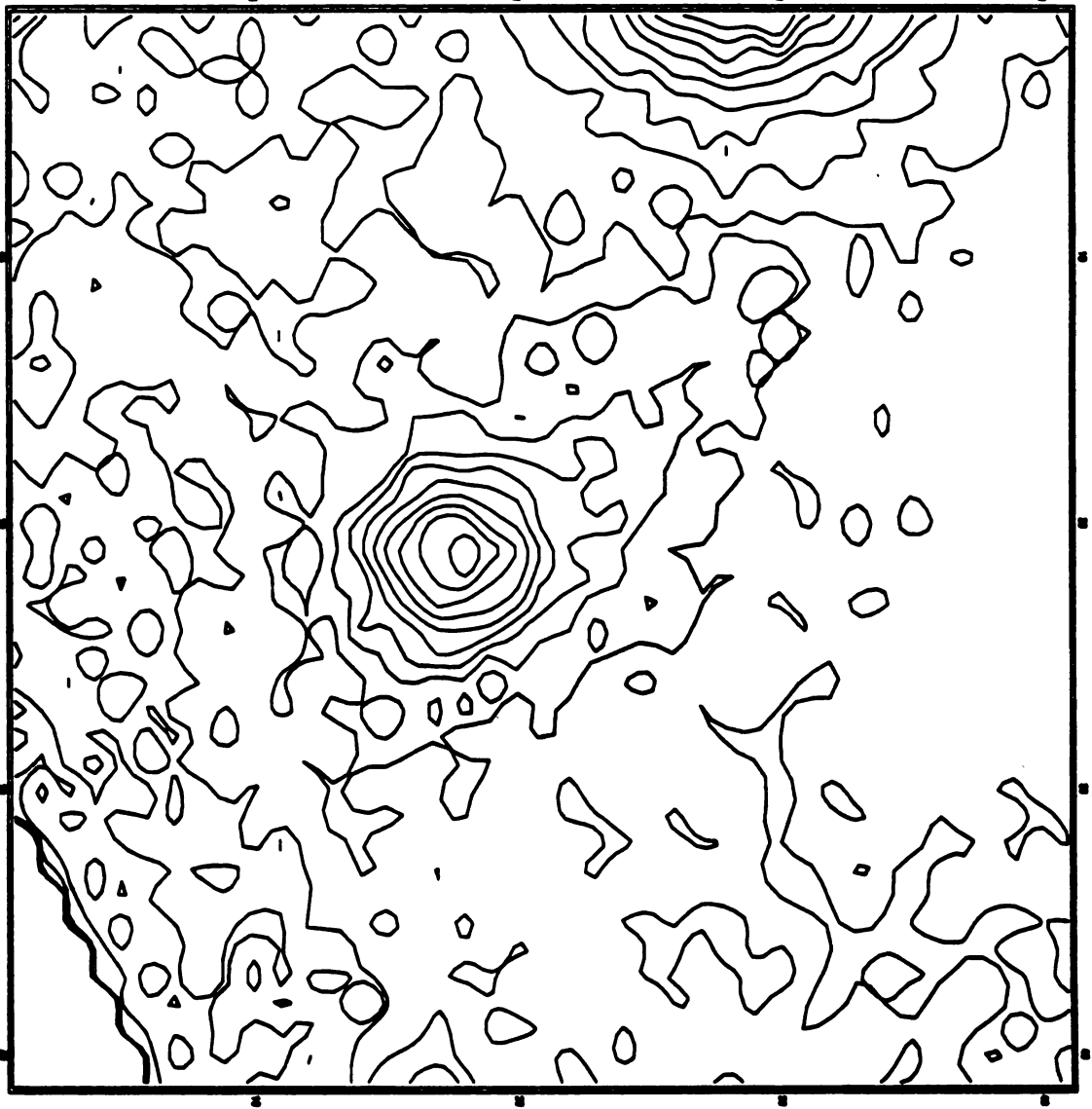


Figure 21 (cont'd): Candidate 2.



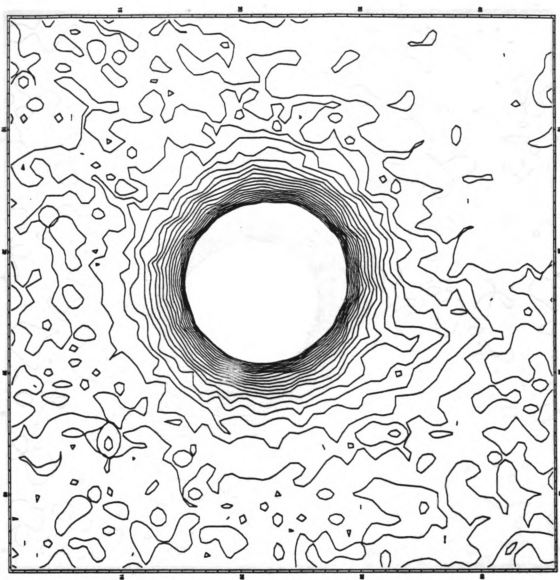


Figure 21 (cont'd): Candidate 3.

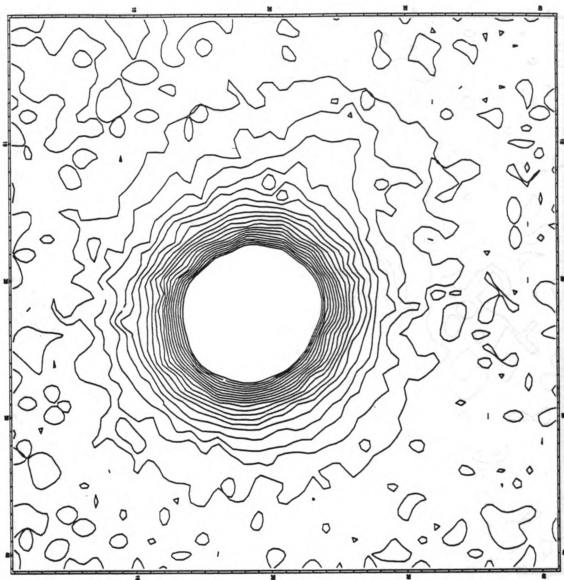


Figure 21 (cont'd): Candidate 4.

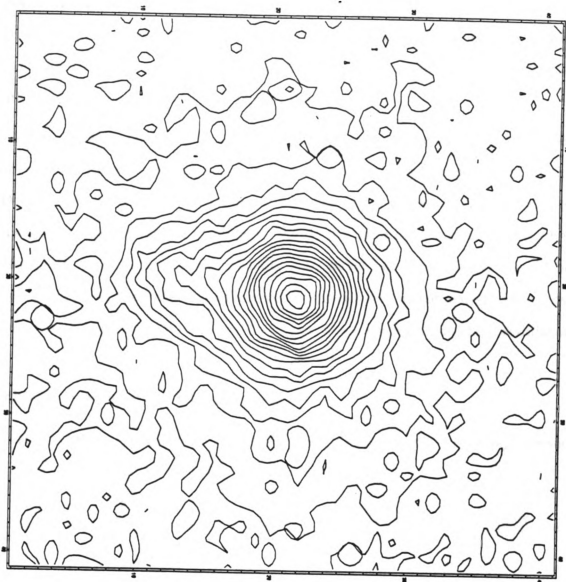


Figure 21 (cont'd): Candidate 5.

around the cD in the plane of the sky. Candidate 4 has a radial velocity above the cDs (970 km/s) closer to the velocity dispersion and a wake that is slightly fainter in relation to the parent galaxy than candidate 3. It is possible that it is orbiting with a smaller component in the plane of the sky.

What is really necessary in this analysis is color. A difference in color between the wake and parent galaxy, i.e. a wake color on par with the local color in the cD envelope and not a continuation of the color of the galaxy profile, would provide strong support for the candidacy. We do not have data available in another wavelength to do this analysis. Equally substantial but more difficult would be measurements of the wake and galaxy velocity dispersion as compared to the local cD envelope dispersion. Without such analysis, these wakes remain only candidates.

**Table 1: Simple Wake Characteristics**

	R(")	DL(A/D units)	$r_g$ (")	$l_w$ (")	$m_g(\text{mag/arcsec}^2)$	$m_w(\text{mag/arcsec}^2)$
1	61.9	13.0	2.9	2.9	15.29	25.21
2	13.5	335.	.80	2.3	18.18	25.25
3	21.9	375.	2.7	2.7	15.87	24.54
4	54.2	48.1	2.7	2.0	16.89	24.87
5	159.	35.3	1.9	2.1	17.99	24.06

## CHAPTER 4

# DISCUSSION

### 4.1 A2670

The smoothness in the diffuse envelope in A2670 is evident in the fact that we see no departure from the de Vaucouleurs' profile as far as we can trace it. Oemler (1973) reports a measurement of the green surface brightness profile out to 750 kpc ( $H_0 = 50 \text{ km/s/Mpc}$ ). Figure 22a shows a de Vaucouleurs' fit (solid line) to Oemler's data (points) taken from his Figure 4. Figure 22b shows Oemler's data (crosses) and a de Vaucouleurs' fit (dashed line) to our data (points). It is evident from these figures that his measurements from photographic plates are contaminated by scattered light. If this correction were made, his faintest measurement (roughly 29 green mag/arcsec<sup>2</sup>) of the diffuse light would have come at roughly 300 kpc, instead of 750 kpc. We measure a scattered-light-corrected red profile out to a radius of 460 kpc, which is a fair extension of Oemler's measurement capabilities.

Another point for comparison is the percentage of the diffuse light to the total cluster light. Our measurement yields approximately  $30 \pm 8\%$ , where the uncertainty is mostly due to our uncertainty in background corrections. Oemler reports 35%, though he considers the envelope to be separate from the elliptical core of the cD galaxy. He arrived at this number by calculating the scale factor that will allow his envelope to match his cluster profile (see his figure 6, the scale factor being roughly 0.27). By assuming that the diffuse light is a percentage of the cluster light

(i.e.  $10^{0.27}$  diffuse light = cluster light), he computes the ratio of the diffuse light to diffuse light plus cluster light to be 0.35. We do not confirm this—the diffuse light follows the total cluster light for approximately  $1'$  and then clearly declines more rapidly with radius.

We must address the notion of the halo as separate from the cD. There has been work done (Schombert 1988) in which clusters were identified to have diffuse light by an apparent break in the cD's surface brightness profile. Before the break, the profile belongs to the parent galaxy, and after the break, it belongs to the envelope. According to Schombert, this characteristic break in the profile occurs around  $24 \text{ V mag/arcsec}^2$ . We see no such break in the profile of A2670 in either R- or V-bands, although the profile is not well fit by any common function for radii less than  $8''$ , and this is roughly the point the V-band profile becomes brighter than  $24. \text{ mag/arcsec}^2$ . We contend that the cD and its envelope or the diffuse light are one entity.

The smoothness of this halo implies that the ICM is well-homogenized, suggesting that it was formed during the initial cluster collapse. Also (following Merritt's argument), matter stripped by galactic collisions should move in orbits coincident with those of the colliding galaxies. This implies that the density profile of the stripped matter should be more centrally concentrated than that of the galaxies as the time for stripping to occur depends strongly on the galaxy density. Though we found that the diffuse light extends about a factor of two less than Oemler quotes, it is still hard to invoke collisions as producing the smooth halo radii beyond 3 core radii where the density has already fallen by a factor of 2.

What is the source of the intra-cluster light or cD halo ? Our limits on the variance-to-mean diffuse light ratio suggest the number of sources per pixel is large ( $\geq 7.5 \times 10^3$ ). The luminosity of each source is less than  $3.0 \times 10^3 L_{\odot}$ , which is about a

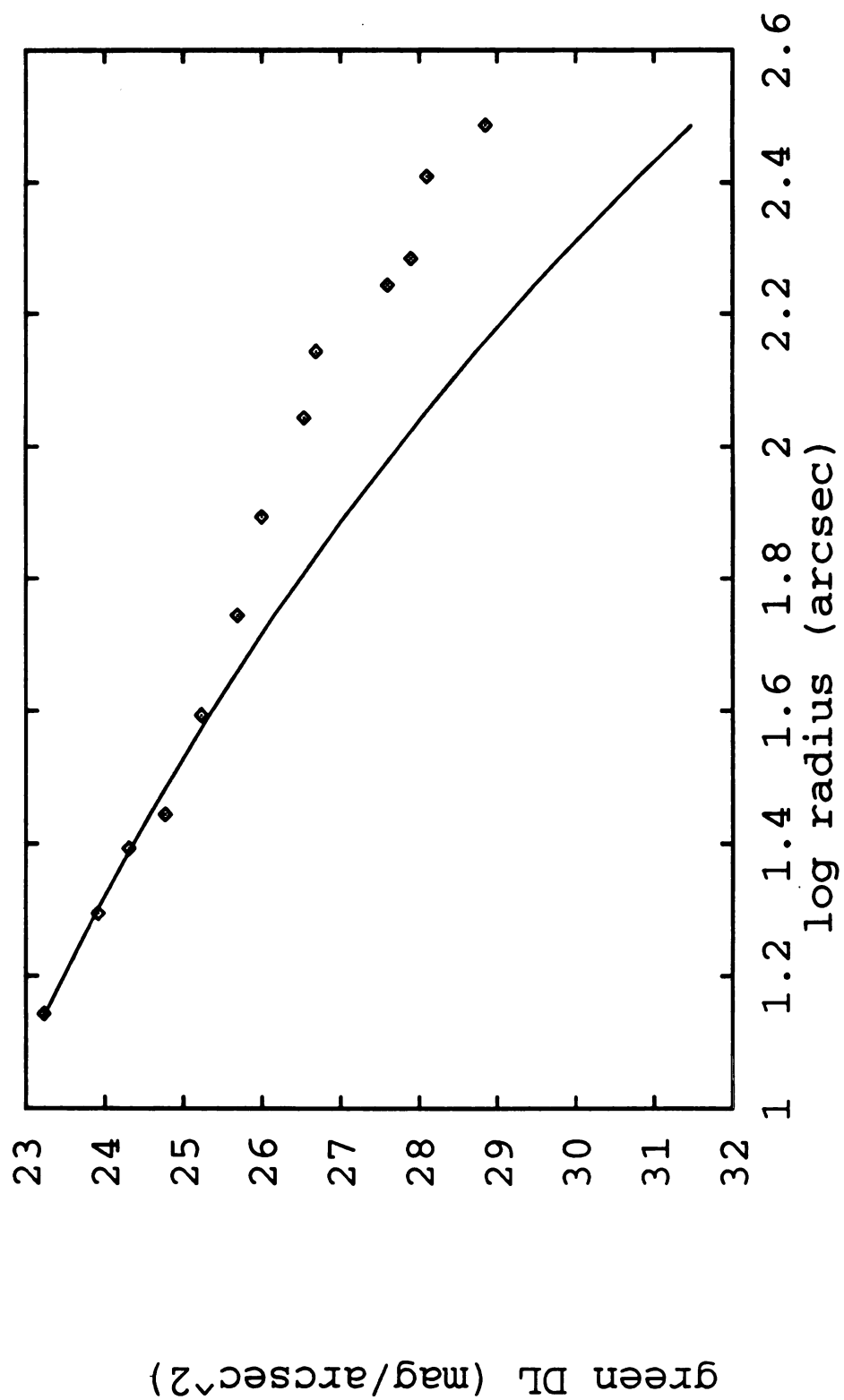


Figure 22a: De Vaucouleurs' Fit to Oemler's A2670 Diffuse Light Measurement.

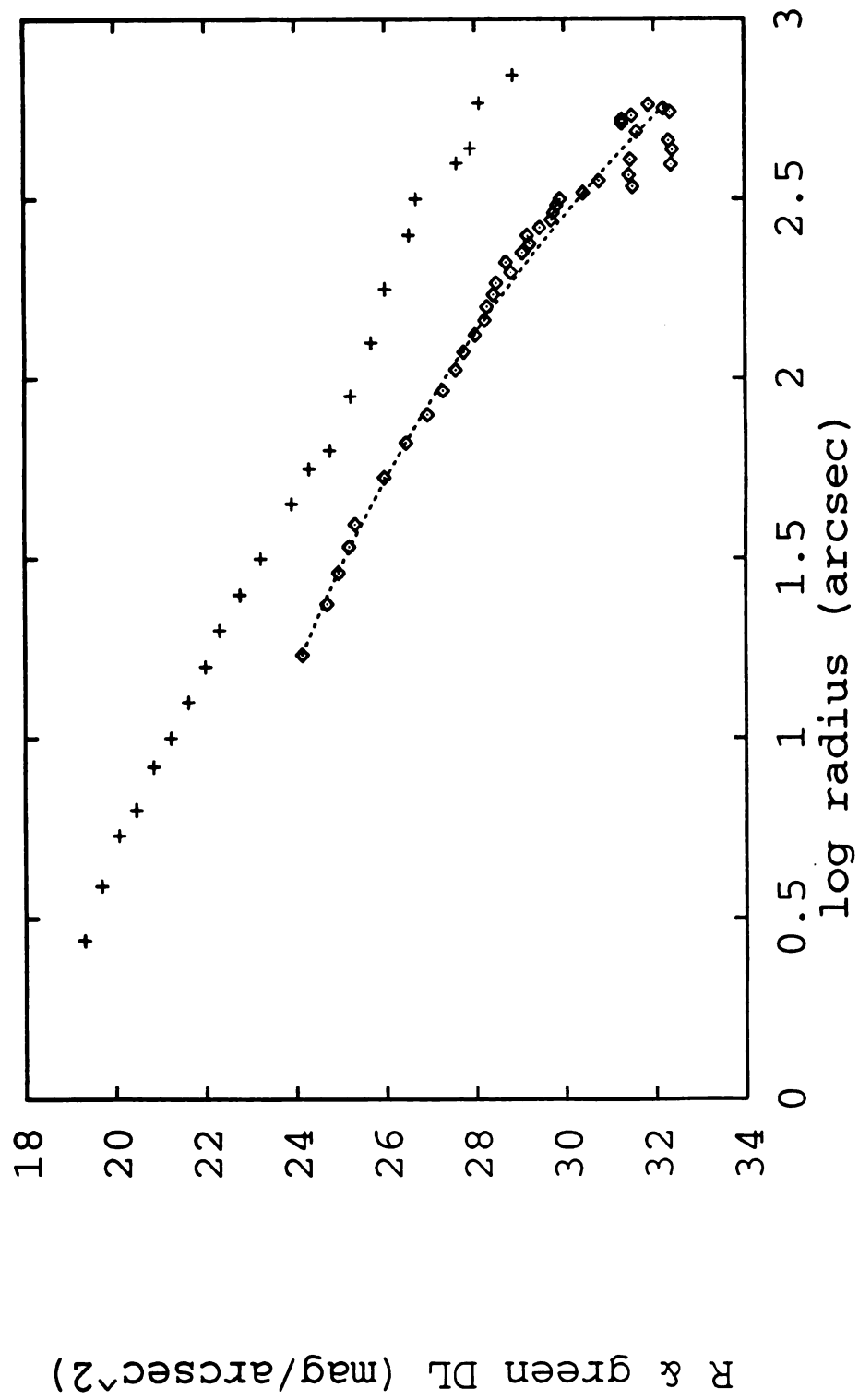


Figure 22b: Oemler's & De Vaucouleurs' Fit to Our Diffuse Light Measurement.



factor of a hundred smaller than the luminosity of the faintest dwarf galaxies. This suggests that the source of the diffuse light is stars, not faint unresolved galaxies.

Dressler (1978a) determined the LF of A2670 from photographic plates. Unfortunately a direct comparison is impossible as we do not have sufficiently accurate background measurements. Our DLF does suggest that there is a shortage of faint objects (or overabundance of bright ones) within the extent of the halo. Our number density of objects does not resemble the diffuse light profile. The diffuse light signal is not large enough for the statistical noise level near the cluster center to selectively obscure faint objects in the central region. We also do not see a significant increase in the number density of bright objects in the center so as to attribute the lack of faint galaxies to obscuration. A deficit of faint galaxies might be caused by two things. As the cluster tidal field is larger in the center, the fainter galaxies might have been tidally stripped. If mergers are more prevalent in the center (because the density is higher) then more bright galaxies could be expected to live there, though the current number density distribution (that we measure at this epoch) does not reflect a great central enhancement. Alternatively, the apparent excess of bright objects may be simply due to mass segregation, that is, brighter heavier objects falling to the center due to dynamical friction.

One interesting question we can ask of the apparent deficit is whether or not there are enough missing objects to account for the diffuse light. If we integrate the DLF, i.e. the number of objects per pixel weighted by the luminosity, we find that the faint objects fail to account for the diffuse light by about 2 orders of magnitude. Surprisingly, the excess light from the bright objects is approximately the same order of magnitude as the diffuse light.

The color gradient of the halo is a potentially very interesting diagnostic. It

could tell us how well the cluster is mixing material stripped from galaxies. It could give information on the age of the central versus outer regions of the ICM, as well as indicate possible regions of star formation. We can compare our estimate of the halo color gradient with the range of values found by Mackie et al. (1990) for the innermost regions of 14 central dominant galaxies. Considering only the cD morphological type, the change in V-R color per kpc ranges between -0.002 to 0.013. For BM class 1, they find the average V-R gradient to be  $0.000 \pm 0.002$  mag/kpc. These gradients were derived out to a maximum radius of 20 kpc ( $h = 1/2$ ). In these units, our gradient is  $-0.003(\pm 0.001)/\text{kpc}$ , which we measure over roughly 210 kpc. Another comparison may be drawn with Mackie's (1992) g-r measurements of cD envelopes extending out to roughly  $1'$ . For the 3 cD's studied (A2589, A2634, and A407), the author reports no evidence of excessive blue colors in the envelope, while for A2589, the envelope becomes 0.2 mag redder than the nucleus at large radii. Also, Schombert (1988) measured the B-V color of 3 cD galaxies (NGC 6034, A1767-G1, and A1414-G1) and reported no evidence of strong color gradients or blue envelopes. However, blueward gradients have been found in 5 out of 6 of the cDs studied by Valentijn (1983). For A496, he finds roughly a 0.6 mag drop in the B-V color over  $2'$  along the semi-major axis. This is the same rough drop we see in V-R for A2670.

The interpretation of color gradients by means of analysis of stellar populations implies the sorting of various age and composition sub-populations. The lack of a priori knowledge about the ages of the star populations in cD galaxies and the metallicity abundances makes analysis of the color gradients difficult. Blue halos are expected in models in which the cD halos are formed from remnant material of tidal interactions on the spiral galaxies in clusters (Ostriker 1977). This scenario

does not explain the observed very red nuclei of cDs (Valentijn 1983, Mackie 1992 and references therein). Metal abundances are thought to influence the observed colors of star populations in two ways. First when the metallicity of a given star on the giant branch is increased, the effective temperature of the star is decreased leaving its bolometric luminosity unchanged (Rood 1972). Tinsley (1978) estimated the B-V color increases by 0.25 when the metallicity is increased from 0.01 to 0.04, while Mould (1991) estimated the V-I color increases by 0.28. This color variation is not enough to explain the color gradient reported here or by Valentijn. Secondly, the appearance of hot horizontal branch stars in old metal poor populations affects the color. However this phase is relatively short in a star's evolution (O'Connell 1982), and therefore the fractional contribution of the horizontal branch light in a normal old metal population is small and never dominates in R- and V-bands (Rabin 1980, Iben & Renzini 1983). The color-spectral index relation (Faber 1977, Sandage and Visvanathan 1978, McClure et al. 1980) indicates that less luminous galaxies are bluer and have lower metal indices and has often been interpreted as the effect of metallicities on color. However, on the basis of an inverse correlation in the line strength between the Balmer lines and the metallic lines in galactic nuclei, Heckman (1980) has shown that the less luminous galaxies are bluer because of the presence of a young stellar populations.

It seems plausible that the color gradient in the cDs indicate ongoing star formation as a consequence of gas-accretion processes. In this interpretation, the radial color distribution should reflect the different rates of star formation and/or radial dependence of the initial mass function of star formation. The detected light in the cD halos should be a mixture of young and old stars. The young stars will dominate the B-V, hence it is feasible to interpret the B-V gradients in terms of the properties

of a young population. The V-R color may represent more of a mixture. It might be interesting to pursue observations of the halo color in the infrared with the hope of learning more about the distribution of the older halo star population.

The focus of this study was to measure any departures of the diffuse light profile from the smooth de Vaucouleurs' profile. The autocorrelation has proven to be our most sensitive probe. It has also allowed us to extract a potentially useful spatial scale. Unfortunately, our two different methods of removing the diffuse light in A2670 have not yielded comparable numbers (3" or 14"), though we are confident we are measuring a signal not found in the outermost regions of the cluster. This number describes a characteristic size of the clumpiness of the material giving rise to diffuse light fluctuations. These clumpings may well be unresolved galaxies in the center of the cluster, although as we described earlier the diffuse light is much too smooth to be composed entirely of unresolved galaxies.

If the autocorrelation gives a measure of the physical extent of the inhomogeneities in the diffuse light, can these clumpings give us an estimate on the age of the cluster ? That is, can we determine the timescale for an initial inhomogeneity to evolve to the scale we measure ? If we have a clump in the density distribution we can describe its motion with the continuity equation. Here we imagine the diffuse light to be a relaxed group of background orphan stars which are on approximately random trajectories such that they have a null group velocity, and the clump has a group velocity resembling that of the galaxy it was stripped from. It is not difficult to show that the lifetime of the inhomogeneity goes as the time to orbit the cluster. This once again suggests that the diffuse light is not currently being formed as it takes far too long for inhomogeneities to smooth out.

On the other hand, these clumpings may represent the LF below our detection

limit. Our rough calculation of this contribution to the autocorrelation yields results that are on the same order as what is observed (ignoring the unknown size of the contributing objects). However, there is evidence that the LF function in the center of A2670 is abnormal; i.e. there is a lack of faint objects from what is expected for a Schechter LF. Our rough calculation certainly rules out an large upturn in the faint end of the LF, implying that a Schechter LF is not that poor of a representation for this region of the LF. A more sophisticated analysis, one in which the characteristics of contributing faint galaxies are considered, will be necessary to validate the results of our rough calculation. We might then be able to place tighter constraints on the form of the LF.

Until recently, studies of clusters of galaxies with dominant cDs have found them at the kinematical center of the cluster (Malumuth et al. 1992 and references therein). With the now larger sample of galaxies, several of the clusters have a cD with a peculiar velocity of several hundred kilometers/second. For A2670, the peculiar velocity is  $439 \pm 119$  km/s. The fact that A2670 and 16 other clusters (although for an alternative perspective see Gebhardt & Beers 1991) with dominant cD's have significant peculiar velocities poses a problem for current models of cluster evolution which require the cluster be not only located at the center of the cluster, but at rest with respect to the cluster as well. Merritt's tidal truncation scenario would make fast work of any large elliptical that spent a significant time away from the center. Another problem arises in how the diffuse light can remain smooth if it is either attached to and moving with the cD at the peculiar velocity or if it is somehow fixed and the cD is moving through it.

We did a simple calculation of the damping time for a cD in a external potential. The cD is bouncing back and forth within a tidal radius with an initial velocity of

the peculiar velocity. We chose two forms for density distribution of the ICM: either homogeneous with a density

$$\rho_o = \frac{9\sigma^2}{4\pi G r_o^2}$$

where  $\sigma$  is the velocity dispersion,  $G$  the gravitational constant, and  $r_o$  is the radius at which the density falls to half its central value (taken as the cluster core radius), or a King density profile

$$\rho(r) = \frac{\rho_o}{(1 + r^2/r_o^2)^{3/2}}.$$

A constant density gives rise to a harmonic oscillator force density,  $-4\pi G \rho_o r/3$ , while the King density yields a more complicated expression for the force density, but roughly equivalent results. We solve the following equation using a fifth order Runge Kutta method (Press et al. 1992):

$$\frac{dv_M}{dt} = -4\pi \ln(\Lambda) G^2 M \frac{\rho}{v_M^2} \left[ \text{erf}\left(\frac{v_M}{\sqrt{2}\sigma}\right) - \sqrt{\frac{2}{\pi}} \frac{v_M}{\sigma} e^{-\frac{v_M^2}{2\sigma^2}} \right] + a(r).$$

The first term is Chandrasehkar's dynamical friction formula (Binney & Tremaine 1987) where  $v_M$  is the velocity of mass  $M$ ,  $\ln \Lambda$  is the coulomb logarithm, and  $\text{erf}$  is the error function. The second term is either expression for the external force density. The constants were chosen to be  $\sigma = 880$  km/s,  $r_o = 160$  kpc,  $M = 10^{13} M_\odot$ , and  $\rho_o = 5.0 \times 10^6 M_\odot/\text{kpc}^3$ . We make the following note on the choice of mass: the  $M/L$  of  $\sim 3$  for galaxies and an absolute  $V$  magnitude of -25.2 for the cD (Oemler 1973) yields a lower cD mass bound of  $M = 3 \times 10^{12} M_\odot$ . Alternatively, Oemler quotes a total mass for the cluster of  $1.12 \times 10^{15}$  to  $1.89 \times 10^{15} M_\odot$  from velocity dispersion measurements and a cluster  $M/L$  of 150 to 255  $M_\odot$ . Given the diffuse light-to-total light ratio, it appears that  $10^{13} M_\odot$  is a reasonable lower limit to the cD mass. For the coulomb logarithm, we use our cD mass choice (the mass of an

ICM constituent being negligible), a maximum impact parameter of a core radius, and a velocity far from the impact of the cluster velocity dispersion. With these values,  $\ln \lambda$  is about 1.

We want to estimate the damping time for the cD. Is this the same as the cluster age ? We are assuming that the cD has somehow already formed and has become caught in the tidal field. In this scenario, its peculiar velocity is either left over from the formation process or it resulted from some impulsive interaction with another body. If it is the former case, the damping time must be roughly the age of the cluster for us to observe an anomolous velocity; if it is the latter, the interaction had to happen long enough ago such that the halo could re-homogenize. As we showed before, that timescale is roughly the orbital time of a test particle within the cluster, which is  $\sim 10^9$  yrs. For a range of initial distance from the cluster center  $\leq r_o$  and velocity  $\leq \sigma$ , the damping time was consistently  $2 \times 10^9$  to  $3 \times 10^9$  yrs.

Malumuth (1992) has run more sophisticated N-body simulations in order to understand the distribution of cD galaxy peculiar velocities. He also found that cD's form in poor clusters (100 galaxies) from the general population (after roughly 9 mergers) and relax to the center in about  $3 \times 10^9$  yrs. The modeled distribution of peculiar velocities viewed at a cluster age of  $10^{10}$  yrs differs significantly from the observed distribution: it is hard to make enough cD's with high peculiar velocities due to the efficiency of dynamical friction and two-body relaxation.

What about the possibility of sub-clustering in A2670 ? As discussed by Sharples et al. (1988), A2670 may be contaminated by a foreground sub-cluster. They model this possibility with a primary cluster having the systematic velocity of the cD and a secondary lower velocity component. With the entire sample of 220 galaxies, they can rule out this hybrid model with any choice of component sizes

to a confidence interval of  $\geq 95\%$  level using the Kolmogorov-Smirnov test, except when the components are equal. They also consider and rule out the possibility of a clump of galaxies centered on the cD itself. (Although using mixture modelling techniques, Bird 1993 reports a four-group split as the "statistically preferred model." Three of the four groups have position centroids consistent with each other within the  $1\sigma$  interval implying that a merging event may be occurring along the line-of-sight to the system.) The picture favoured by us (and Sharples et al. 1988) is one in which the cD galaxy formed relatively early in the cluster's evolution; the presence of a substantial peculiar velocity for the cD indicates the mixing process is not yet complete. If there really is sub-clustering in A2670, we will then have an even harder task to explain the smoothness of the diffuse light in the presence of interacting sub-clumps.

## 4.2 A2029

UBK showed that the diffuse light profile followed a de Vaucouleurs' profile out to 425/h kpc. Although we do not go out as far and do not correct for scattered light, we confirm the smoothness in the diffuse light profile. UBK also report that the isophotes have a constant ellipticity 0.90 at all radii. With slightly better resolution data, it is apparent that the ellipticity increases to 1. for radii less than 20".

According to Schombert's (1988) classifications, A2029 is technically not cD because it does not have a diffuse light envelope as characterized by the inflection in the surface brightness profile. The velocity dispersion measurements as function of radius (Dressler 1979) also show no inflection. Both suggest that the cD and diffuse light are one entity.

Dressler (1979) also found no evidence of rotation within 30 kpc of the center



of the cD, but reports tentative results of rotational velocity of 100-200 km/s in the outermost regions. Even if this rotation is real, comparison with the velocity dispersion indicates that the cD is not supported primarily by rotation, as is the case in elliptical galaxies. However, work by Bower et al. (1988) suggests there is structure in the velocity field; i.e. there exists a segregation of galaxies with slightly positive velocities from those with slightly negative velocities. The authors suggest two possible explanations. First, there may exist a sub-clump superimposed on the core of A2029, which is not unlikely given the nature of hierarchical clustering. Second, the entire system is rotating. This is contrary to the "classical" picture of cluster structure as the high velocity dispersion implies that the cluster core is not in virial equilibrium. However, this effect may occur if the cluster has formed by the decay of the a binary cluster.

The surface brightness fluctuation measurements also indicate that the source of the diffuse light is numerous ( $\geq 300$ ) low luminosity ( $\leq 3 \times 10^5 L_{\odot}$ ) objects. The autocorrelation results indicate again that there is some clumpiness of material with spatial scale  $\sim 17''$  more prevalent near the center of the cluster. What is new for this cluster is 5 wake candidates. Extremely deep optical images were necessary for the detection; the features were just visible on our data frame with 1.5 times less S/N. Without color or velocity data, we have no confirming evidence that these features are really the wakes formed by the parent galaxy passing through the diffuse light. Until those measurements are made, numerical simulations can be run to calibrate the response of the diffuse light. This would allow a determination of the mass of the impinging galaxy. We could check this mass determination against that obtained with measurements of the parent galaxies' luminosity and assuming a standard M/L for cluster galaxies.

### 4.3 Concluding Remarks

We argue that the cD envelope is old (greater than  $10^{10}$  yrs) as indicated by its smoothness, but the cD velocity with respect to the cluster center (or the presence of sub-clumps) is evidence for clusters youth (less than  $10^{10}$  yrs). This is a curious problem for cluster evolution models. It will be interesting to perform similar measurements for other cD's with high peculiar velocities to see if they too appear to be falling through the cluster potential, not disturbing its halo as it does so. If all of these clusters also have large cooling flows, indicating that the luminosity is generated on short timescales, the halo velocity would then be decoupled from the cD. Further, more sensitive, measurements of the diffuse light anisotropy may reveal evidence for motion of the cD through the halo or multiple-nuclei interactions. If these measurements show as little inhomogeneity as we report here, the currently favored cluster evolution theories will have to be reconciled with overall smoothness of the diffuse light.

Also of great interest would be further measurements of the velocity dispersion of the diffuse light as function of position in the cluster. This would allow a study of the dynamical anisotropy of the cluster. A continuous velocity dispersion profile (well past the 24-25 mag/arcsec<sup>2</sup> reported inflection point in the surface brightness profile) would aid our understanding of the origin of the diffuse light, i.e. if the inner and outer regions really have a different origin.

Finally, questions concerning the X-ray diffuse light should be addressed in a manner similar to what is discussed here. One might imagine that inhomogeneities (e.g. H $\alpha$  filaments, the "evidence" for cooling flows) in this profile would be correlated with those in the other wavelengths.

## **LIST OF REFERENCES**

## LIST OF REFERENCES

- Abell, G.O. 1958 *Ap.J.Suppl.* **3** 211.
- Abell, G.O. 1962 in *Problems of Extragalactic Research* ed. G.C. McVittie (Macmillan: New York) p 213.
- Bahcall, N.A. 1977 *Ann.Rev.Astr.Ap.* **15** 505.
- Bahcall, N.A. 1981 *Ap.J.* **247** 787.
- Baum, W.A. 1973 *P.A.S.P.* **85** 530.
- Beers, T.C. & Geller, M.J. 1983 *Ap.J.* **274** 491.
- Binggeli, B. 1982 *A.&A.* **107** 338.
- Binney, J. & Tremaine, S. 1987 *Galactic Dynamics* (Princeton University Press: Princeton)
- Bird, C.M. 1993 *Ap.J.* Accepted.
- Blakeslee, J.P. & Tonry, J.L. 1992 *Ap.J.* **103** 1457.
- Blanford, R.D. & Smarr, L. 1982 Preprint.
- Bothun, G.D. & Schombert, J.M. 1988 *Ap.J.* **335** 617.
- Bower, R.G., Ellis, R.S. & Efstathiou, G. 1988 *M.N.R.A.S.* **234** 725.
- Burnstein, D. & Heiles, C. 1982 *A.J.* **87** 1165.
- Carlberg, R.G. 1984 *Ap.J.* **286** 403.
- Carter, D., Inglis, I., Ellis, R.S., Efstathiou, G. & Godwin, J.G. 1985 *M.N.R.A.S.* **212** 471.
- Carter, D. & Metcalfe, N. 1980 *M.N.R.A.S.* **191** 325.

- Chokshi, A. & Wright, E.L. 1987 *Ap.J.* **319** 44.
- Cohen, J.G. 1986 *A.J.* **92** 1039.
- Cowie, L.L. & Hu, E.M. 1986 *Ap.J.* **305** L39.
- Davis, L.E. 1989 "A User's Guide to the IRAF APPHOT Package" *IRAF User Handbook, Volume 2b* NOAO.
- Davies, R.L., Efstathiou, G., Gall, S.M., Illingworth, G. & Schechter, P.L. 1983 *Ap.J.* **266** 41.
- De Vaucouleurs, G. 1948 *An.d'Ap.* **11** 247.
- De Vaucouleurs, G. & de Vaucouleurs, A. 1970 *Ap.Letters.* **5** 219.
- Dressler, A. 1978a *Ap.J.* **223** 765.
- Dressler, A. 1978b *Ap.J.* **226** 55.
- Dressler, A. 1979 *Ap.J.* **231** 659.
- Dressler, A. 1981 *Ap.J.* **243** 26.
- Dressler, A. 1984 *Ann.Rev.Astr.Ap.* **22** 185.
- Fabian, A.C., Nulsen, P.E.J. & Canizares, C.R. 1984 *Nature* **310** 733.
- Faber, S.M., Burstein, D. & Dressler, A. 1977 *A.J.* **82** 941.
- Faber, S.M. 1977 in *Evolution of Galaxies and Stellar Populations* eds. B.M. Tinsley & R.B. Larson (Yale University Observatory: New Haven) p 157.
- Fitchett, M.J. 1988 *M.N.R.A.S* **230** 161.
- Gebhardt, K. & Beers, T.C. 1991 *Ap.J.* **383** 72.
- Gudehus, D.H. 1989 *Ap.J.* **340** 661.
- Gott, J.R. & Thuan, T.X. 1976 *Ap.J.* **204** 649.
- Hausman, M.A. & Ostriker, J.P. 1978 *Ap.J.* **224** 320.
- Hill, J.M., Hintzen, P., Oegerle, W.R., Romanishin, W., Lesser, M.P., Eisenhamer, J.D. & Batuski, D.J. 1988 *Ap.J.* **332** L23.

- Heckman, T.M. 1980 *A.&A.* **87** 142.
- Hoessel, J.G. 1980 *Ap.J.* **241** 493.
- Hoessel, J.G. & Schneider, D.P. 1985 *A.J.* **90** 1648.
- Hu, E.M. 1992 *Ap.J.* **391** 608.
- Hubble, E. 1936 *The Realm of the Nebula* (Yale University Press: New Haven).
- Iben, I., Jr. & Renzini, A. 1983 *Ann.Rev.Astr.Ap.* **21** 271.
- Jones, C. & Forman, W. 1984 *Ap.J.* **276** 38.
- Kuhn, J.R., Lin, H. & Lorz, D. 1991 *P.A.S.P.* **103** 1097.
- Lambas, D.G., Groth, E.J. & Peebles, P.J.E. 1988 *Ap.J.* **95** 996.
- Landolt, A.U. 1983 *A.J.* **88** 439.
- Larson, R.B. 1975 *M.N.R.A.S.* **173** 671.
- Lauer, T.R. 1988 *Ap.J.* **325** 49.
- Lauer, T.R. 1990 in *Dynamics and Interactions of Galaxies* ed. R. Wielen (Springer-Verlag: Heidelberg) p 406.
- Lugger, P.M. 1984 *Ap.J.* **278** 51.
- Maccagni, D., Garilli, B., Gioia, I.M., Maccaro, T. Vettolani, G. & Wolter, A. 1988 *Ap.J.* **334** L1.
- Mackie, G. 1992 *Ap.J.* **400** 65.
- Mackie, G., Visvanathan, N. & Carter, D. 1990 *Ap.J.Suppl.* **73** 637.
- Malumuth, E.M. 1983, Ph.D. Thesis, University of Michigan.
- Malumuth, E.M. 1992 *Ap.J.* **386** 420.
- Malumuth, E.M. & Kirshner, R.P. 1981 *Ap.J.* **291** 8.
- Malumuth, E.M. & Richstone, D.O. 1984 *Ap.J.* **276** 413.
- Malumuth, E.M., Kriss, G.A., Van Dyke Dixon, W., Ferguson, H.C. & Ritchie, C. 1992 *A.J.* **104** 495.

- Malumuth, E.M., Smith, E.P. & Kriss, G.A. 1989 *B.A.A.S.* **21** 1168.
- Matthews, T.A., Morgan, W.W. & Schmidt, M. 1964 *Ap.J.* **140** 35.
- McClure, R.D., Cowley, A.P. & Crampton, D. 1980 *Ap.J.* **236** 112.
- McHardy, I. 1978 *M.N.R.A.S.* **184** 783.
- McGlynn, T.A. & Ostriker, J.P. 1980 *Ap.J.* **241** 915.
- McNamara, B.R. & O'Connell, R.W. 1989 *A.J.* **98** 2018.
- McNamara, B.R. & O'Connell, R.W. 1992 *Ap.J.* Accepted.
- Melnick, J., White, S.D.M. & Hoessel, J.G. 1977 *M.N.R.A.S.* **180** 207.
- Merrifield, M.R. & Kent, S.M. 1991 *A.J.* **98** 351.
- Merritt, D. 1984a *Ap.J.* **276** 26.
- Merritt, D. 1984b *Ap.J.* **280** L5.
- Merritt, D. 1985 *Ap.J.* **289** 18.
- Morgan, W.W. 1958 *P.A.S.P.* **70** 364.
- Morgan, W.W. & Lesh, J.R. 1965 *Ap.J.* **142** 1364.
- Mould, J.R. 1991 in *The Stellar Populations of Galaxies* 149<sup>th</sup> IAU Symposium, eds. B. Barbuy & A. Renzini (Kluwer: Dordrecht) p 181.
- Mulder, W.A. 1983 *A.&A.* **117** 9.
- O'connell, A. 1982 *Ap.J.* **209** 89.
- Oemler, A., Jr. 1973 *Ap.J.* **180** 11.
- Oemler, A., Jr. 1974 *Ap.J.* **194** 1.
- Oemler, A., Jr. 1976 *Ap.J.* **209** 693.
- Ostriker, J.P. & Hausman, M.A. 1977 *Ap.J.* **217** L125.
- Ostriker, J.P. 1977 in *Evolution of Galaxies and Stellar Populations* eds. B.M. Tinsley & R.B. Larson (Yale University Observatory: New Haven) p 369.

- Ostriker, J.P. & Tremaine, S.D. 1975 *Ap.J.* **202** L113.
- Peletier, R.F., Davies, R.L., Illingworth, G.D., Davis, L.E. & Cawson, M. 1990 *A.J.* **233** 62.
- Persson, S.E., Grogel, J.A. & Aaronson, M. 1979 *Ap.J.Suppl.* **39** 61.
- Press, W.H, Teukolsky, S.A., Vetterling, W.T. & Flannery, B.P. 1992 *Numerical Recipes in Fortran, 2<sup>nd</sup> ed.* (Cambridge University Press: Cambridge).
- Porter, A.C. 1988 Ph.D. Thesis, California Institute of Technology.
- Quintana, H. & Lawrie, D.G. 1982 *A.J.* **87** 1.
- Rabin, D.M. 1980 Ph.D Thesis, California Institute of Technology.
- Rhee, G.F.R.N. & Katgert, P. 1987 *A.&A.* **183** 217.
- Rhee, G.F.R.N. & Roos, N. 1990 *M.N.R.A.S.* **243** 629.
- Romanishin, W. 1987 *Ap.J.* **323** L113.
- Rood, H.J. & Leir, A.A. 1979 *Ap.J.* **231** L3.
- Rood, H.J. 1972 *Ap.J.* **177** 681.
- Sandage, A. 1972 *Ap.J.* **178** 1.
- Sandage, A. & Hardy, E. 1973 *Ap.J.* **183** 743.
- Sandage, A. & Visvanathan, N. 1978 *Ap.J.* **223** 707.
- Sarazin, C.L. 1988 *X-Ray Emmissions from Clusters of Galaxies* (Cambridge University Press: Cambridge).
- Sarazin, C.L., O'Connell, R.W. & McNamara, B.R. 1992 *Ap.J.Let.* Submitted.
- Sastry, G.N. 1968 *P.A.S.P.* **80** 252.
- Schechter, P.L. 1976 *Ap.J.* **203** 297.
- Scheick, X. & Kuhn, J.R. 1993 *Ap.J.* Accepted.
- Schombert, J.M. 1984 Ph.D. thesis, Yale University.
- Schombert, J.M. 1987 *Ap.J.Suppl.* **64** 643.



- Schombert, J.M. 1988 *Ap.J.* **328** 475.
- Schneider, D.P., Gunn, J.E. & Hoessel, J.G. 1983 *Ap.J.* **268** 476.
- Sharples, R.M., Ellis, F.S. & Gray, P.M. 1988 *M.N.R.A.S.* **231** 479.
- Smith, R.M., Efstathiou, G., Ellis, R.S., Frenk, C.S. & Valentijn, E.A. 1985 *M.N.R.A.S.* **216** 71P.
- Struble, M.F. 1987 *Ap.J.* **317** 668.
- Struble, M.F. & Peebles, P.J.E. 1985 *Ap.J.* **90** 582.
- Struble, M.F. & Rood, H.J. 1982 *A.&A.* **87** 7.
- Tammann, G.A., Yahil, A. & Sandage, A. 1979 *Ap.J.* **234** 775.
- Tonry, J.L. 1983 *Ap.J.* **266** 58.
- Tonry, J.L. 1984 *Ap.J.* **279** 13.
- Tonry, J.L. 1986 *A.J.* **90** 2431.
- Tonry, J.L. 1987 in *Structure and Dynamics of Elliptical Galaxies*, 127<sup>th</sup> IAU Symposium, ed. T. de Zeeuw (Reidel: Dordrecht) p 89.
- Tonry, J.L. & Schneider, D.P. 1988 *A.J.* **96** 807.
- Thuan, T.X. & Kormendy, J. 1977 *P.A.S.P.* **89** 466.
- Thuan, T.X. & Romanishin, W. 1981 *Ap.J.* **248** 439.
- Tinsley, B.M. 1978 *Ap.J.* **222** 14.
- Tremaine S. 1989 in *Dynamics and Interactions of Galaxies* ed. R. Wielen (Springer-Verlag: Berlin) p 394.
- Uson, J.M., Boughn, S.P. & Kuhn, J.R. 1991 *Ap.J.* **369** 46.
- Valentijn, E. 1983 *A.&A.* **118** 123.
- Van Albada, T.S. 1982 *M.N.R.A.S.* **201** 939.
- Weinberg, M.D. 1989 *M.N.R.A.S.* **239** 549.
- White, S.D.M. 1980 *M.N.R.A.S.* **191** 1P.
- Zwicky, F. 1938 *P.A.S.P.* **50** 218.

MICHIGAN STATE UNIV. LIBRARIES



31293010222598